UDC 551.465.7:551.513.13:551.511.33

CLIMATE AND THE OCEAN CIRCULATION

II. THE ATMOSPHERIC CIRCULATION AND THE EFFECT OF HEAT TRANSFER BY OCEAN CURRENTS

SYUKURO MANABE

Geophysical Fluid Dynamics Laboratory, ESSA, Princeton, N.J.

ABSTRACT

A general circulation model of the joint ocean-atmosphere system is constructed by combining an ocean model and an atmospheric model. The quantities exchanged between the oceanic part and the atmospheric part of the joint model are momentum, heat, and water. Integration of the atmospheric part yields the surface wind stress, net radiation, sensible heat flux, rates of rainfall and snowfall, rates of evaporation and sublimation, and rates of runoff and iceberg formation, all of which constitute the upper boundary conditions for the oceanic part of the model. From the oceanic part, the thickness of ice and the distribution of sea-surface temperature, which constitute the lower boundary conditions for the atmospheric part of the model, are computed.

An approach toward a quasi-equilibrium state of the joint ocean-atmosphere system is attempted by numerical time integration of the joint model. Since the thermal relaxation time of the oceanic part of the model is much longer than that of the atmospheric part, a special technique for economizing the computation time is developed. Although a state of quasi-equilibrium is not reached satisfactorily, the time variation of the atmospheric "climate" is extremely slow toward the end of the time integration. A detailed analysis of the final solution at the end of the integration is carried out.

According to this analysis, the distributions of various heat balance components such as radiation flux and the turbulent flux of sensible and latent heat compare favorably with the corresponding distributions in the actual atmosphere estimated by Budyko and London.

By comparing the final state of the joint model atmosphere with the quasi-equilibrium state of the previous atmosphere without an active ocean, it is possible to identify the effect of an ocean circulation on the general circulation of the atmosphere. For example, the poleward transport of heat by an ocean circulation reduces the meridional gradient of atmospheric temperature and vertical wind shear in the troposphere. This reduction of vertical wind shear lowers the level of baroclinic instability and causes a general decrease in the magnitude of eddy kinetic energy in the atmosphere. The air mass modification by the energy exchange between the model ocean and atmosphere creates a favorable place for the development of cyclones off the east coast of the continent in high latitudes.

In the Tropics, the upwelling of relatively cold water at the Equator suppresses the intensity of rainfall in the oceanic region and increases it in the continental region. This increase significantly alters the hydrology of the tropical continent. In middle and subtropical latitudes, the advection of warm water by the subtropical gyre increases the flux of sensible and latent heat from the ocean to the atmosphere along the east coast of the continent and increases the intensity of precipitation in the coastal region. The subtropical desert of the joint model is more or less confined to the western half of the continent. In high latitudes, the advection of warm water by the subarctic gyre off the west coast of the continent increases the energy exchange and precipitation there. Most of these modifications contribute to make the hydrology of the joint model highly realistic despite the idealization of the land-sea configuration.

CONTENTS

1. INTRODUCTION

As we explained in the introduction to part I, the major objective of this part of our three-part study is to identify the various roles of ocean circulation in maintaining the climate of the atmosphere.

The basic method of approach adopted for this investigation is to compare

1) the state of the model atmosphere reached by the numerical integration of the joint ocean-atmosphere model and

2) the quasi-equilibrium state that emerged from the numerical integration of the "atmosphere-only" model, analyzed and discussed extensively in part I.

The difference between these two states should suggest how the ocean circulation influences the thermal and dynamical structure and the hydrology of the atmosphere.

For ease of identification, we shall refer to the joint ocean-atmosphere model as the "joint model" and the atmospheric model without any ocean circulation as the "A-model."

2. STRUCTURE OF THE JOINT MODEL

In the continental region, the joint model is identical to the A-model, described in part I. In the oceanic region, the effect of the ocean circulation is incorporated by combining the ocean circulation model with the general circulation model of the atmosphere. Figure 1, a box diagram, indicates the coupling among the major components of the joint model. Since these major components are explained in parts I and III (Manabe, 1969, and Bryan, 1969), we shall concentrate on describing the link between the atmospheric part and the oceanic part of the joint model. The quantities exchanged between ocean and atmosphere are heat, water, and momentum. These three fluxes will be discussed in the following subsections.

Heat exchange—In the A-model, the heat capacity of the ocean as well as of land is assumed to be zero, and the temperature of the ocean surface is computed from the condition of heat balance among net radiation and the turbulent flux of sensible and latent heat. In the joint model, the temperature of the ocean surface is determined from the thermodynamical equation involving the effect of advection by the ocean currents (part III). This temperature constitutes the lower boundary condition for the atmospheric part of the model. The various heat balance components listed above constitute the source or sink term for the thermodynamical equation presented in part III. The distribution of albedo of the ocean surface for solar radiation, chosen for this study, is given in part I.

When ice covers the sea surface, it is necessary to compute the temperature of the ice surface from the condition of heat balance. The equation of heat balance at the ice surface may be expressed by

$$S_*+(\mathrm{DLR})_*=\sigma T_*^4+({}_vH)_*+({}_vLH)_*+({}_0\mathrm{H})_*$$

where S_*, $(\mathrm{DLR})_*$, $({}_vH)_*$, and $(VLH)_*$ are net downward solar radiation, downward long-wave radiation, turbulent flux of sensible heat, and the turbulent flux of latent heat at the ice surface, respectively. $({}_0\mathrm{H})_*$ is the downward conduction of heat through ice and is explained in detail in part III. For the computation of net solar insolation, the albedo of ice is assumed to be 0.7. Further details of the heat balance equation may be found in subsection 2E of part I. Once the temperature of the ice surface T_* is determined so that it satisfies the heat balance equation, it is then possible to compute the magnitude of the downward conductive flux of heat $({}_0\mathrm{H})_*$, which constitutes the heat source term for the thermodynamical equation of sea water under the ice.

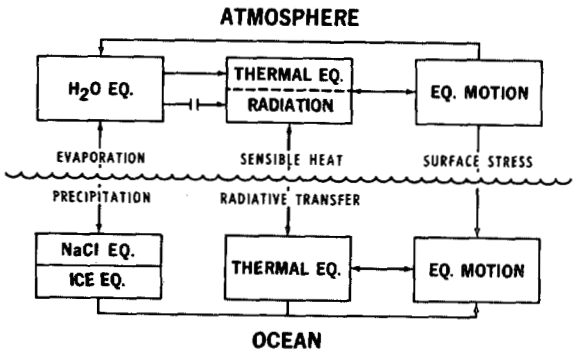

FIGURE 1.—Box diagram of the joint model structure.

Water exchange—In the joint model, the exchange of water and ice between ocean and atmosphere or between ocean and continent affects the distribution of salinity and sea ice in the ocean. Therefore, it is necessary to compute the magnitudes of these exchanges in order to predict the distributions of salinity and of sea ice.

Figure 2 shows the various components of the hydrologic cycle and the coupling among these components in the joint model. As this figure indicates, the ocean gains water either through rainfall, runoff from the continent, or the melting of sea ice, and loses water either through evaporation, sublimation, or the freezing of water. The salinity of sea water is diluted or concentrated depending upon whether the ocean gains or loses water. This figure also shows that the amount of sea ice increases either through snowfall, iceberg formation, or freezing, and decreases through sublimation or melting. Since the methods of predicting the distribution of salinity and of sea ice are described in detail in part III, they are not discussed here. Instead, we shall describe how the distributions of flow of runoff and of icebergs into the ocean are determined.

As we described in part I, the runoff takes place when the amount of soil moisture tends to exceed the field capacity of soil. The amount of runoff reaching the coastline is controlled by the direction of riverflow. Figure 3 shows the pattern of riverflow chosen for this study. In the continental domain A, water flows from west to east and supplies the water to the western shore of the ocean (E). In the continental domain B, however, water flows from east to west and reaches the eastern shore of E. The water supply from domain C is distributed uniformly to the coastline of C.

In order to prevent the snow from accumulating indefinitely, we introduced a highly idealized mechanism of iceberg formation. If the snow depth exceeds a certain critical depth, that is, 20 cm of water equivalent, snow is assumed to form icebergs, which in turn move toward the coastal region and become sea ice. The direction of iceberg movement is assumed to be identical with that of water flow, described above.

As we shall explain later, the atmospheric part of the model is integrated for a period of 365 atmospheric model

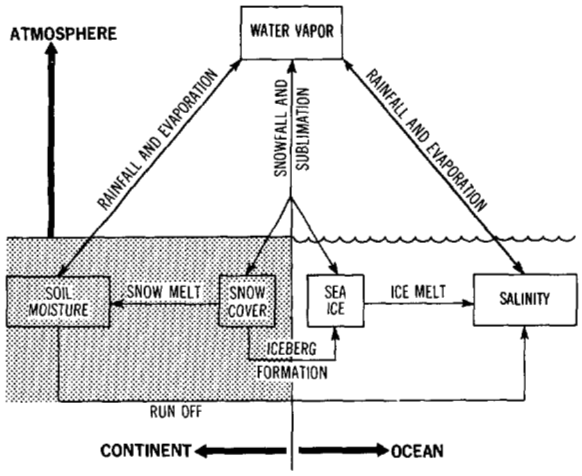

FIGURE 2.—Box diagram of the hydrologic system of the joint model.

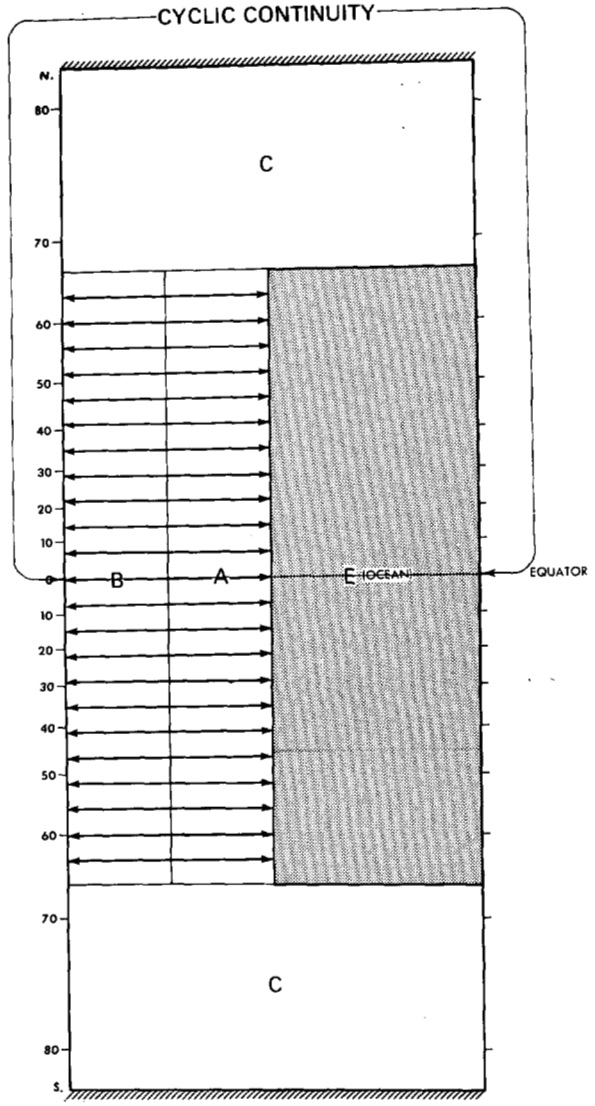

FIGURE 3.—River flow map, corresponding to the computation of runoff in the model.

days. While it is obvious that icebergs cannot form during such short periods, this idealized mechanism of iceberg formation is introduced to obtain a quasi-steady state of the distribution of snow depth.

Momentum exchange—The exchange of momentum [1] is computed from equation (11) of part I. This formula should not (strictly speaking) be used because one must take into consideration the velocity of ocean currents. The velocity of ocean currents, however, is much smaller than the velocity of air flow; for this reason, the effect of ocean currents on the momentum exchange is neglected.

3. METHOD OF APPROACH

As usual, we try to approach the state of quasi-equilibrium asymptotically by numerical time integration of the joint model. The major difficulty in this approach is the extremely long relaxation time involved in the change of thermal structure of the ocean (part III). It takes approximately 6 mo to 1 model year for the atmospheric model to reach a state of quasi-equilibrium; whereas, it may take several hundred years for the oceanic model to reach a corresponding quasi-equilibrium state. Accordingly, the relaxation time of the joint model should be the longer one of the two, that is, several hundred years. Since the atmospheric part of the model requires about 45 min of machine time (UNIVAC 1108) for the time integration of 1 model day, it is unreasonable to perform the integration of the joint model for a period of hundreds of model years. Therefore, we devised an approach designed to economize computer time.

Figure 4 shows schematically the basic principle of this approach. The coupling between the atmospheric part and the oceanic part of the model is adjusted so that the evolution of the former during 1 atmospheric model year is coupled with that of the latter during 100 oceanic model years. For example, the atmosphere on the 0th, 0.5th, and 1st atmospheric year interacts with the ocean on the 0th, 50th, and 100th oceanic year of time integration, respectively. By synchronizing the relaxation time of the former with that of the latter in this way, we hope to optimize the amount of computation required for reaching a state of quasi-equilibrium.[2]

Information concerning sea-surface temperature and the distribution of ice thickness is conveyed from the oceanic part of the model to the atmospheric part. On the other hand, the atmospheric part of the model supplies information on the exchange of heat, water vapor, and momentum to the oceanic part of the model. One might wonder whether the amounts of these quantities that are received by the ocean are inconsistent with those lost by the atmosphere because of the artificial synchronization of time, mentioned above. What is exchanged, however, is

[1] After completion of this study, it was found that the distribution of surface stress experienced by the surface of the model ocean is somewhat different, because of a code error, from the stress computed in the atmospheric part of the model. As demonstrated in the appendix, the effect of this code error does not significantly alter the conclusion described in this paper. Therefore, we decided to publish the results in the original form.

[2] Since the time intervals of numerical time integration of the atmospheric and oceanic parts of the model are 10 min and 166.7 min, respectively, such a synchronization implies a 16-step integration of the oceanic part of the model for every 1-step integration of the atmospheric part of the model. In practice, for computational convenince, the computation of 108 steps of the oceanic integration alternated with that of 18 steps of the atmospheric integration.

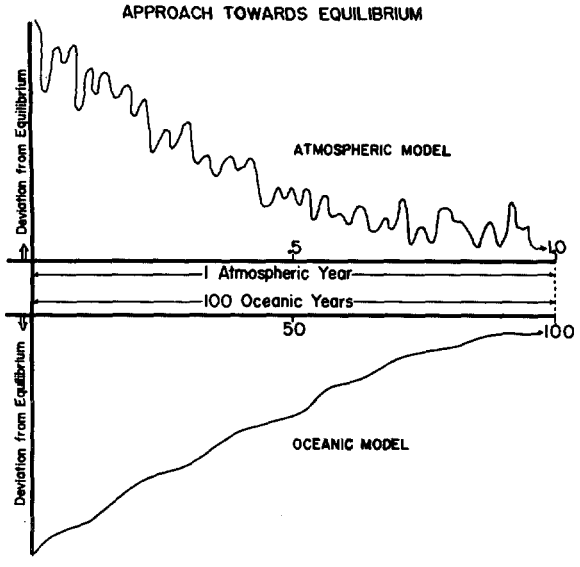

FIGURE 4.—Basic principle of the time integration of the joint model.

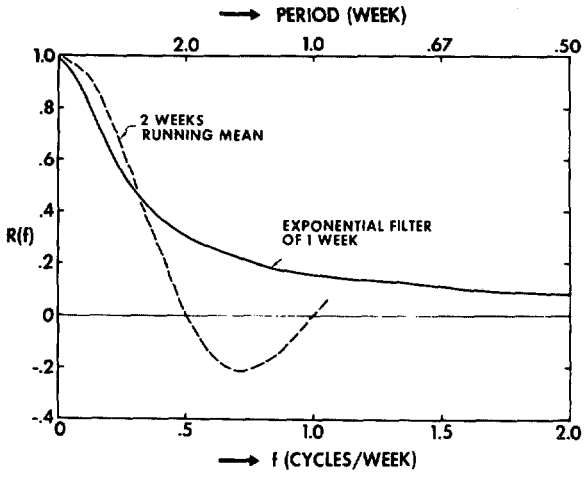

FIGURE 5.—Frequency response $R(f)$ of the exponential filter with a time constant of 1 week (solid line) compared with a running mean of 2 weeks (dashed line).

not the actual amount of these quantities but information on the rate of exchange of these quantities. Therefore, no inconsistency arises.

One of the difficulties arising from this synchronization of two different time scales is the distorted response of the oceanic circulation to fluctuations of atmospheric circulation. For example, it takes about 1 week for a cyclone wave to traverse the oceanic region. Because of the synchronization, the oceanic part of the model would feel this cyclone for as long as 2 oceanic model years; it is, therefore, probable that transient ocean circulations appear. In order to avoid this difficulty, a time-smoothing operator is used on the time series of the rates of exchange of all quantities that the atmospheric part of the model communicates to the oceanic part. This time-smoothing operator is an exponential filter with the weight function $w(t)$.

$$w(t)=\begin{cases}0, & t>0\\ \lambda^{-1}e^{t/\lambda}, & t\leq 0\end{cases}$$

where λ is the so-called time constant chosen for present purposes to be 1 week. Because of the impracticality of storing a large number of long time series in the computer, the filtered series is calculated by an alternate but equivalent method. The exponentially smoothed time series may be obtained from the time series of any quantity q by repeated application of the following formula.

$$\tilde{q}^{\tau}=\frac{\lambda-\Delta t}{\lambda}\tilde{q}^{\tau-1}+\frac{\Delta t}{\lambda}\tilde{q}^{\tau}$$

where $\tilde{\ }$ indicates the smoothed quantity, the suffix τ indicates the τth value in the time series, and Δt is the time interval between the times of two consecutive data. In figure 5, the frequency response of this exponential filter is compared with that of a 2-week running mean. According to this figure, the degrees of smoothing by these two filters are comparable. For further details, see the discussion of smoothing and filtering of time series by Holloway (1958) and Panofsky and Brier (1958).

If the short-period fluctuation of the atmospheric state has a significant effect on the quasi-equilibrium state of the joint system, then the state that we reach by this economical technique is obviously different from the state attained by straightforward integration. In view of the damping effect of the ocean circulation on the short-period fluctuation, the difference between these two states, however, may not be very large. Further study is necessary to prove this point beyond a doubt.

Finally, a diagram summarizing the exchange of information between the two parts of the model is shown in figure 6.

4. INITIAL CONDITION AND TIME INTEGRATION

A. INITIAL CONDITION

The state of quasi-equilibrium that emerged from numerical integration of the A-model, described in part I, is chosen as the atmospheric initial condition.

The oceanic initial condition for the time integration of the joint model is obtained from the numerical integration of the ocean model with a fixed sea-surface temperature. The boundary conditions necessary for this preliminary integration of the ocean model are the sea-surface temperature and the moisture and momentum flux at the sea surface. These values are computed from the quasi-equilibrium state of the A-model atmosphere. In order to get a stable and representative distribution, these quantities are averaged for a period of 100 model days. The details of integration of the ocean model may be found in part III.

Starting from this initial condition, the numerical integration of the joint model is performed. Since this initial condition represents the state of atmosphere and ocean without interaction, the change of the state of the joint system should be caused by the interaction between the ocean and the atmosphere.

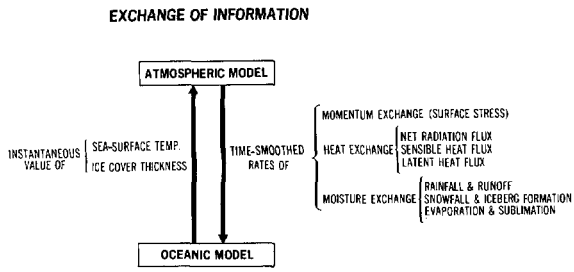

FIGURE 6.—Exchange of information between the atmospheric part and the oceanic part of the joint model.

B. TIME INTEGRATION

The integration of the joint model is performed for a period of 1 atmospheric model year or 100 oceanic model years (see section 3 for explanation of the synchronization of two time scales). The UNIVAC 1108 was used for this computation. The integration of the atmospheric part of the model requires about 300 hr; whereas, that of the oceanic part consumes about 800 hr of machine time. In order to show the gross evolution of the model atmosphere, the time series of mass integrals of some of the fundamental quantities such as total potential energy, area mean value of precipitable water, and total kinetic energy are shown in figure 7. (Note that total potential energy is proportional to the mean temperature of the atmosphere.) This figure clearly shows that the general slope of the potential energy curve tends to level off towards the end of the time integration.

One of the most important quantities determining the interaction between the ocean and the atmosphere is the meridional gradient of sea-surface temperature, for it influences the meridional temperature gradient and, accordingly, the baroclinicity of the atmosphere. In figure 8, the variance of the zonal mean temperature of the surface of the model ocean, which is a good indicator of the meridional gradient of the temperature, is plotted with respect to time. This figure indicates that it changes most markedly during the first 100 atmospheric model days (or the first 28 oceanic years) of the time integration and changes little after this period. Although small net downward heat flux [3] of 0.01 ly min^{-1} from the surface to the interior of the ocean remains toward the end of the time integration (subsection 9B), both figures 7 and 8 indicate that the thermal and dynamical structure of the model atmosphere and the shallower part of the model ocean may not be very far from a quasi-equilibrium state toward the end of the integration. Therefore, it was decided to perform a detailed analysis of the state that emerged from this time integration.

The period of analysis chosen for this study has a span of 100 atmospheric model days, starting from the 260th model day. The data shown in the following sections are obtained by taking the time mean for this 100-day period unless specified otherwise.

[3] Because of this net downward heat flux, the temperature of the deeper part of the model ocean continues to increase with time and does not level off during this time integration. For further discussion of this subject, see part III.

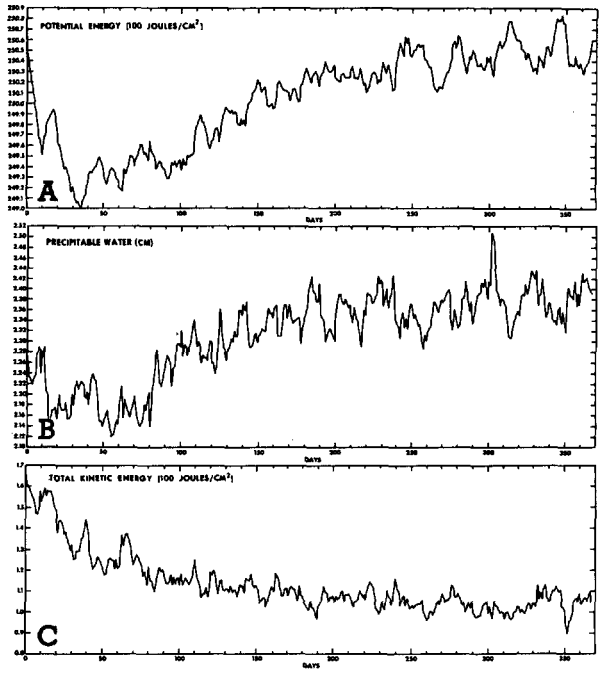

FIGURE 7.—(A) time variation of total potential energy, (B) the areal mean precipitable water, and (C) the areal mean total kinetic energy.

Since the land-sea configuration and the distribution of solar insolation are symmetric with respect to the Equator, the time mean state of the atmosphere is almost symmetric with respect to the Equator. Therefore, the distributions of various quantities in the two hemispheres are usually averaged in order to obtain a sufficient sampling of the data. The hemispheric distributions of various quantities shown in the following sections are obtained by this averaging process unless specified otherwise.

5. TIME MEAN STATE OF THE MODEL ATMOSPHERE

A. THERMAL FIELD

Zonal distribution—The latitude-height distribution of the zonal mean temperature in the joint model atmosphere is shown in figure 9. Since the general qualitative features of this distribution are very similar to those of the A-model atmosphere, we shall not discuss them again here. In order to examine the difference between the thermal structure of the two model atmospheres quantitatively, we obtained the latitude-height distribution of the difference between the zonal mean temperature of two atmospheres. Figure 10 shows the result. As one would expect, the atmospheric temperature of the joint model is generally higher than that of the A-model at high latitudes; whereas the opposite holds true in low latitudes, owing to the effect of heat advection by ocean currents. This general decrease of the meridional temperature gradient has a direct influence on the level of eddy kinetic energy in the atmosphere of the joint model. This subject will be discussed in section 6.

Further examination of the difference shows that, in low latitudes, the cooling effect of the ocean circulation

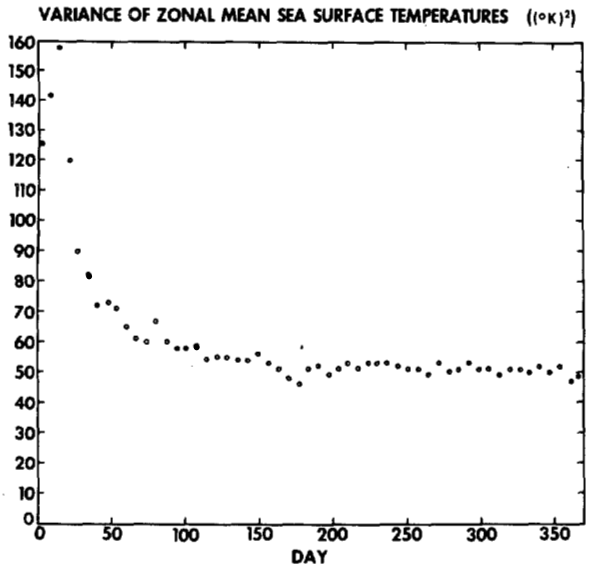

FIGURE 8.—Variance of zonal mean temperature of the ocean surface, plotted with the time interval of approximately 6.7 days.

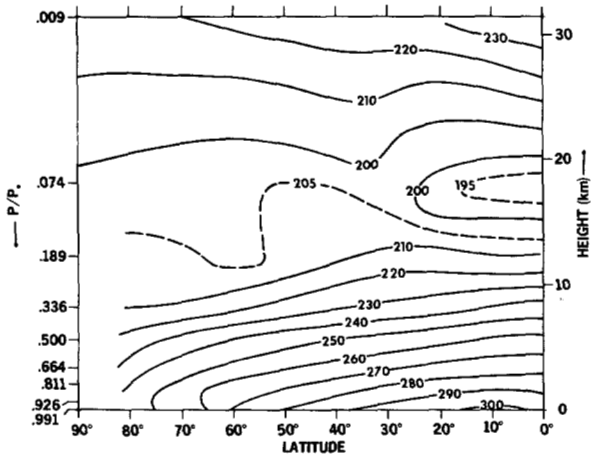

FIGURE 9.—Latitude-height distribution of zonal mean temperature in the joint model atmosphere (°K).

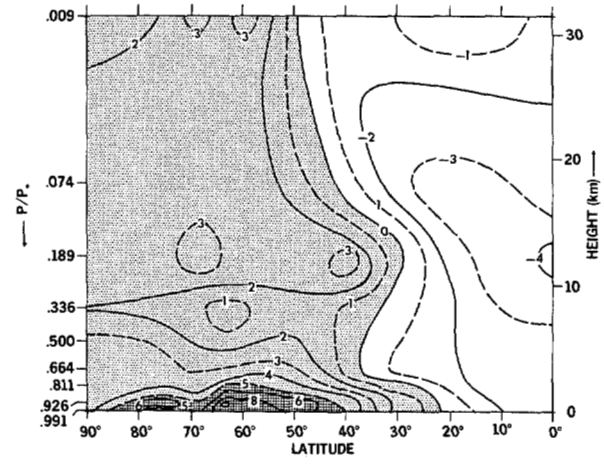

FIGURE 10.—Latitude-height distribution of the difference between the zonal mean temperature of the joint model and the zonal mean temperature of the A-model (°K).

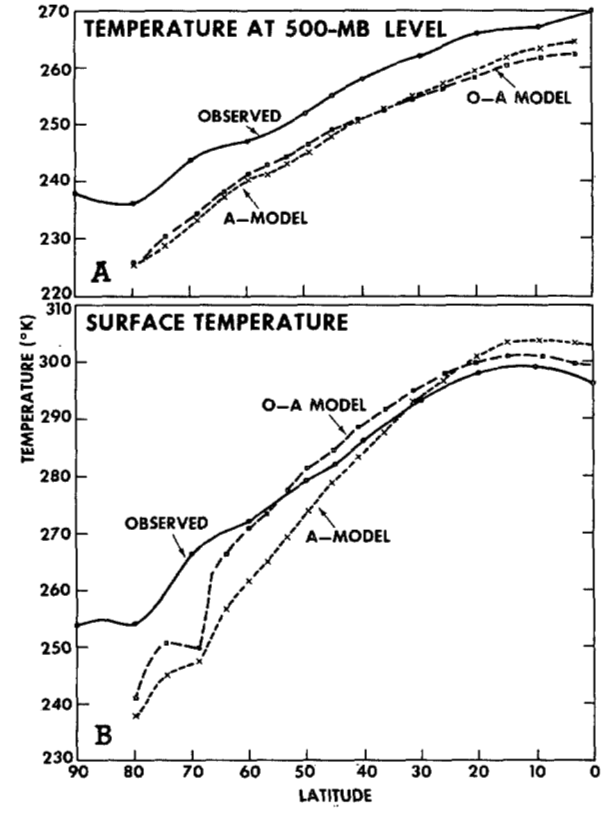

FIGURE 11.—Latitudinal distributions of zonal mean temperature at the (A) 500-mb level and (B) 1000-mb level. Solid line, observed annual mean temperature; dashed line, temperature of the joint model; and dotted line, temperature of the A-model.

extends throughout the troposphere due to the intense convective activity; whereas in high latitudes, the warming effect is limited primarily to the lower troposphere due partly to the static stability of the air mass. Since the warming in the lower troposphere is much more intense than the cooling, the ocean circulation tends to raise the area mean temperature of the lower troposphere and lower that of the upper troposphere.

Figure 11 compares the latitudinal distributions of zonal mean temperature in the model atmospheres with those of the actual atmosphere. Owing to the effect of the ocean circulation, the meridional gradient of surface air temperature of the joint model is much more realistic than that of the A-model except in the polar cap region. The surface temperature in the polar continental cap, however, is too low in the joint model atmosphere as well as in the A-model atmosphere due to the extensive snow cover, which we shall discuss later.

At the 500-mb level of the model atmosphere, the effect of the ocean circulation on the zonal mean temperature is very small. In general, the temperature of both models is several degrees lower than the temperature of the actual atmosphere at this level. The reason for this is not clear.

Areal distribution of temperature—For comparison, the areal distribution of temperature at the earth's surface, for both the joint model and the A-model, is shown in

figure 12. In the oceanic region, the sea-surface temperature of the joint model has a tropical minimum and subtropical maximum due to the effect of upwelling of cold water at the Equator. On the other hand, the sea-surface temperature of the A-model has a maximum at the Euqator. As we shall discuss later, this difference in sea-surface temperature has a profound effect on the hydrologic cycle of the atmosphere. In the middle-latitude region, the meridional gradient of the temperature of the ocean surface is significantly less for the joint model than for the A-model, owing to the poleward transport of heat by ocean currents. The distribution of sea-surface temperature of the A-model is highly zonal in middle latitudes; whereas, that of the joint model increases toward the east. The mechanism of maintaining such a sea-surface temperature will be discussed in part III.

In the continental region, the difference between the distributions of the two models is much less. In the continental part of the tropical rain belt, the temperature of the soil surface is relatively low for both models due to the effect of the evaporation from the wet surface of the soil. This belt of tropical minimum is more pronounced in the joint model than in the A-model because of the difference in the intensity of tropical rainfall which we shall discuss in subsection 8D. In the subtropics of the A-model, the temperature of the soil surface is very high in most of the continental region; whereas in the subtropics of the joint model, it is highest in the western half of the continent due to the increase of rainfall and soil moisture in the eastern half of the continent, an effect of the ocean circulation. In short, for the joint model, the hot desert in the subtropics is more or less limited to the western half of the continent. Further discussion of the subtropical desert is contained in section 8.

Figure 13 shows how the ocean circulation altered the distribution of the air temperature near the earth's surface. In the right-hand part of the figure, the temperature difference between the two models at the lowest model level is shown. As a reference, the temperature distribution of the joint model at the same model level is shown in the left-hand part of the figure. In this figure, the area of maximum difference in the surface air temperature is located in the oceanic region of high latitudes. In this area, the magnitude of positive difference, that is, the temperature increase due to the ocean circulation is as large as 15°C. This rise of temperature results in the large temperature gradient along the ocean-continent boundary in high latitudes and reminds us of the large temperature contrast observed along the coast of the Antarctic Continent.

Despite the moderate rise of temperature due to the effect of the ocean current, the surface air temperature over the high-latitude region of the continent is still much colder than the annual mean surface temperature of the actual atmosphere. As we discussed in part I, one of the

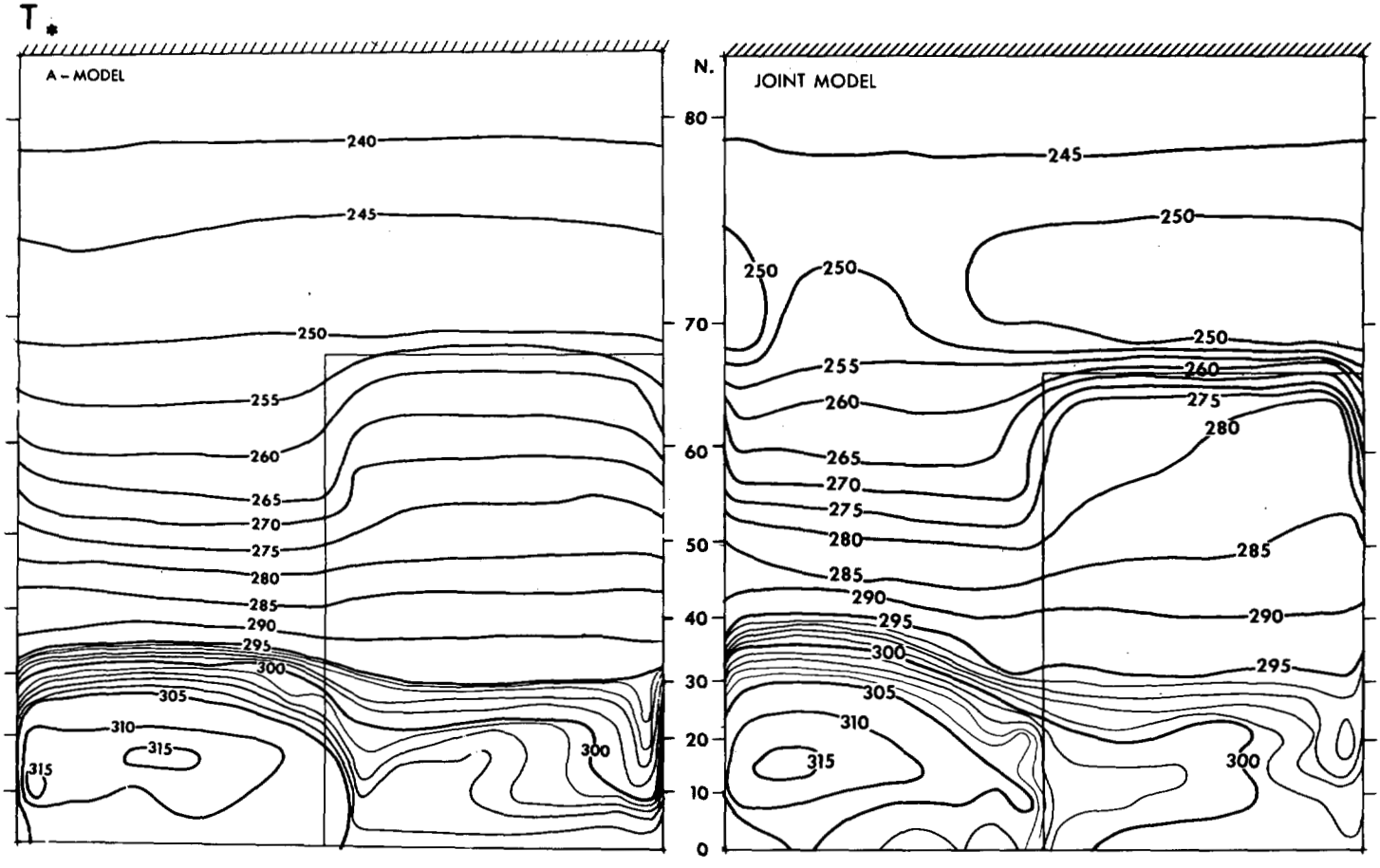

FIGURE 12.—Areal distributions of temperature (°K) of the earth's surface (ocean surface or soil surface).

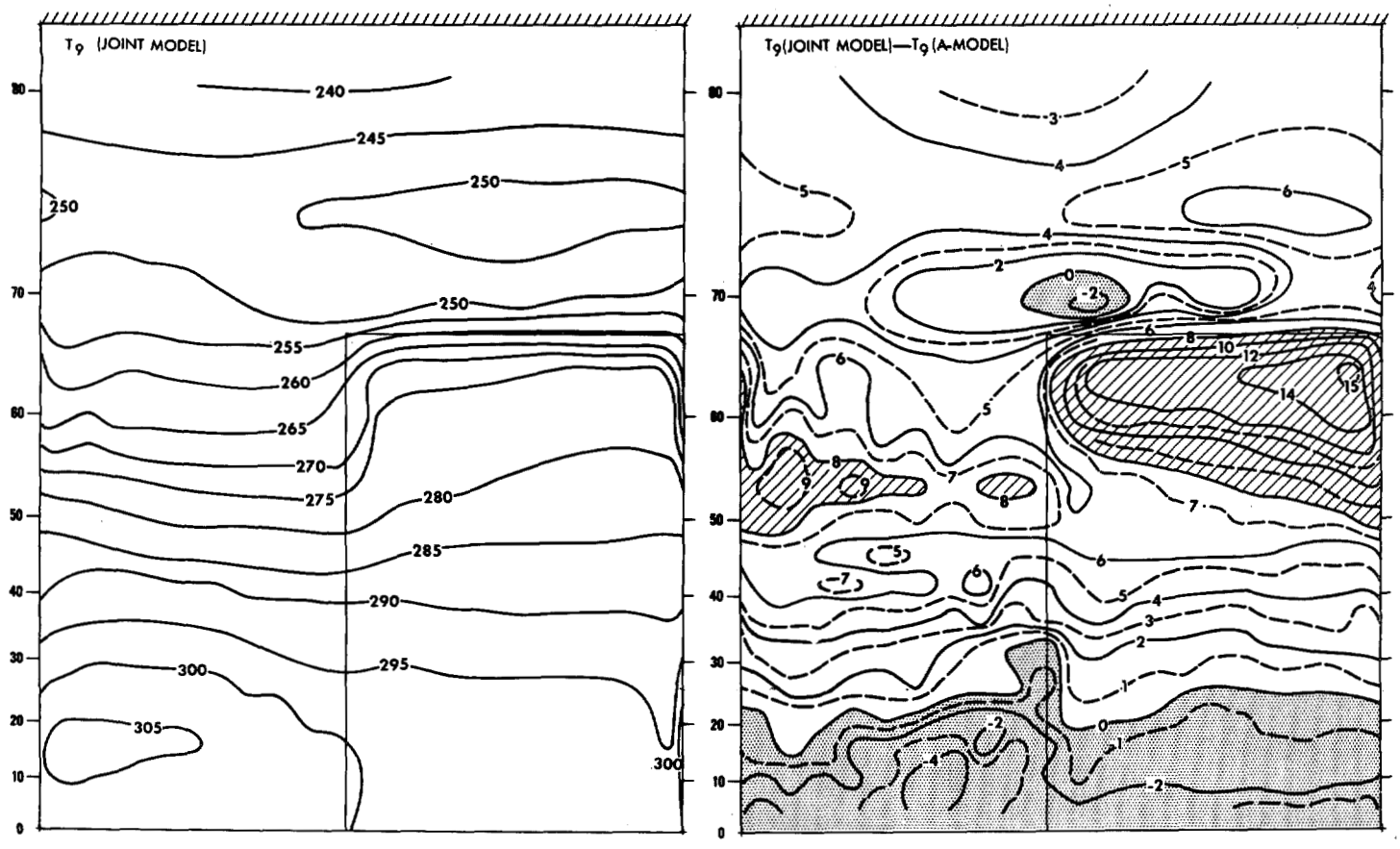

FIGURE 13.—Areal distributions of temperature (°K) at the lowest model level ($P/P_* = .991$) of the joint model and the difference between the temperature of the joint model and the temperature of the A-model at the lowest model level.

major reasons for this discrepancy is the excessive growth of snow cover in the polar region of the continent. We shall discuss this subject in subsection 8E.

In the upper layer of the model atmosphere, the distribution of temperature is highly zonal. Figure 14 shows the areal distribution of temperature at the fifth model level (approximately 500 mb). There are, however, slight longitudinal variations in the middle latitudes, that is, temperature is somewhat lower over the continent than over the ocean.

B. MOISTURE FIELD

The areal distributions of the relative humidity at the lowest level of both the joint model and the A-model are compared in figure 15. One of the major differences between the two distributions lies in the location of the dry zone in the subtropical region of the continent. According to this comparison, the ocean circulation seems to be responsible for eliminating the arid zone in the eastern half of the continent and limiting it to the western half. Note that the area of low relative humidity in the subtropics coincides very closely with the area of high soil temperature shown in figure 12.

Another difference in the distribution is the appearance of a relatively dry zone just poleward of the boundary of the joint model ocean. Such a zone is also discernible in the A-model, but is much less pronounced. It is highly probable that this zone is produced by the local meridional circulation cell, which is enhanced by the large temperature contrast between the ocean and polar cap continent. Unfortunately, the resolution of the finite-

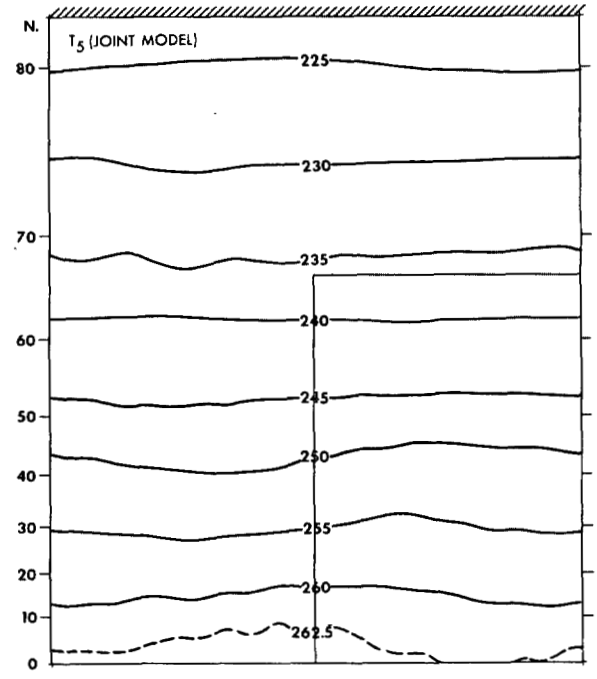

FIGURE 14.—Areal distribution of temperature (°K) at the fifth level ($P/P_* = 0.500$) of the joint model.

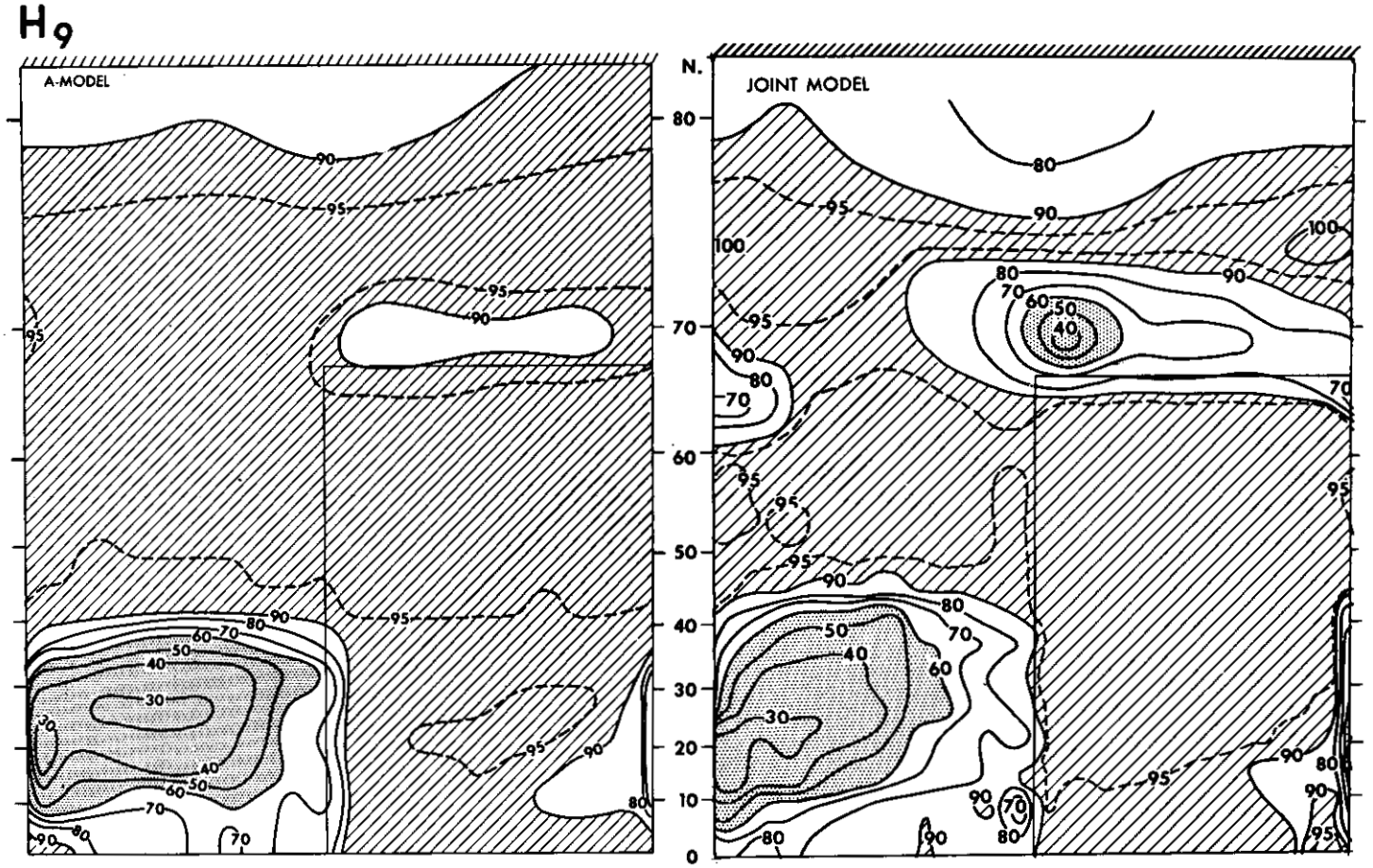

FIGURE 15.—Areal distributions of relative humidity (percent) at the lowest model level ($P/P_* = .991$).

difference grid is not sufficient to resolve this feature in detail and therefore to completely establish its validity. Further investigation of this feature must await more refined calculation.

The latitude-height distribution of zonal mean relative humidity of the joint model is shown in figure 16. This is very similar to the corresponding distribution of the A-model, shown in figure 15 of part I and not discussed here.

C. ZONAL WIND

The latitude-height distribution of the zonal mean of zonal wind in the joint model atmosphere is shown in figure 17A. In order to compare this distribution with that of the A-model, the zonal wind velocity of the A-model is subtracted from the zonal wind velocity of the joint model. The latitude height distribution of the difference is given in figure 17B. The intensity of the zonal wind in the joint model atmosphere is weaker than in the A-model atmosphere equatorward of 55° latitude. The general decrease of the meridional temperature gradient results in a decrease of vertical wind shear and, accordingly, a weakening of the westerlies. Because of this decrease, the stratospheric jet shifts poleward by about several degrees latitude (compare fig. 17A with fig. 10A of part I). The decrease of the vertical wind shear due to the effect of the oceanic heat advection is responsible for the lowering of the level of eddy kinetic energy discussed in section 6. Poleward of 55° latitude, the intensity of zonal wind does not necessarily decrease; between 55° and 70° latitude, it increases due to the effect of ocean circulation. This increase results from the increase of temperature contrast between the cold polar continent and the warm ocean surface surrounding it.

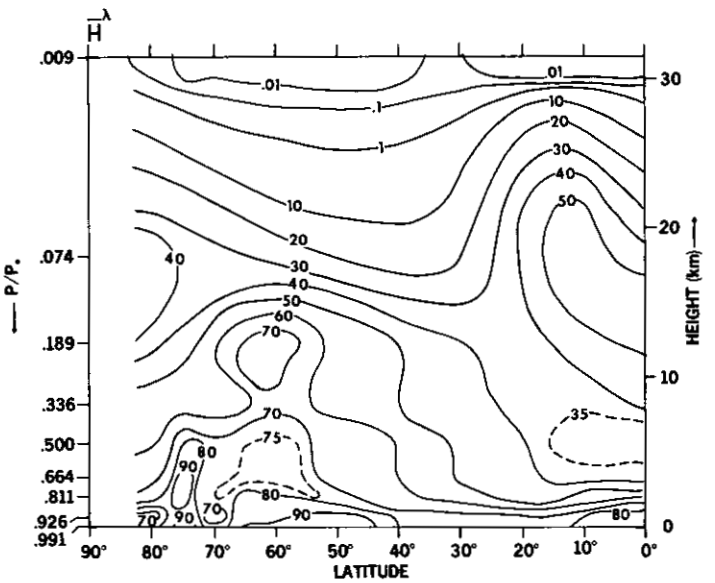

FIGURE 16.—Latitude-height distribution of zonal mean relative humidity (percent) in the joint model atmosphere.

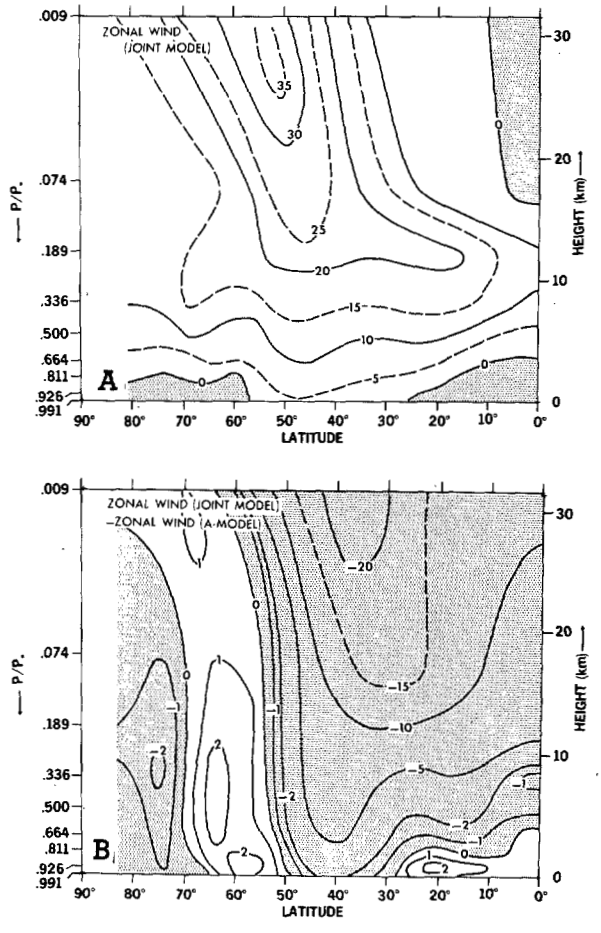

FIGURE 17.—(A) latitude-height distribution of the zonal mean of zonal wind in the joint model atmosphere; (B) zonal mean of the zonal component of wind of the joint model minus that of the A-model. Units, m sec^{-1}.

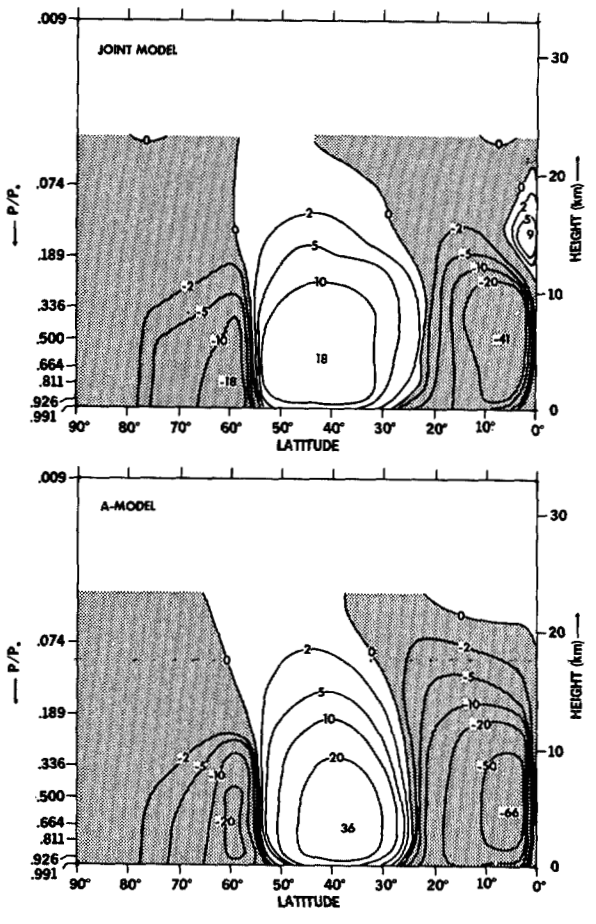

FIGURE 18.—Stream functions of the meridional circulation of the joint model and of the A-model. Units, 10^{12} gm sec^{-1}.

D. MERIDIONAL CIRCULATIONS AND VERTICAL *P*-VELOCITY

The distributions of stream functions of the zonal mean of the meridional circulation in the joint model and the A-model atmosphere are shown in figure 18. In this figure, the three-cell circulation that consists of the direct cell of the Tropics, the indirect cell of the middle latitude, and the direct cell in the polar region appears in both model atmospheres. The intensities of the tropical cell and the indirect cell of the joint model are significantly weaker than those of the A-model. The weakening of the tropical cell resulted from the suppression of the tropical rain belt by the equatorial belt of cold sea-surface temperature discussed in subsection 8A, while the weakening of the indirect cell is consistent with the decrease of eddy kinetic energy in middle latitudes discussed in section 6. The influence of the ocean circulation upon the meridional circulation and the field of vertical motion is also evident in figure 19, which shows the horizontal distributions of the vertical mean, time mean vertical *P*-velocity of both models. For example, the belt of intense upward motion that appears in the oceanic region around the Equator of the A-model is absent in the joint model. Instead, the area of upward motion is limited to the continental region of the joint model Tropics. This result is consistent with the general weakening of the direct Hadley cell mentioned above. In middle and subtropical latitudes, upward motion takes place off the east coast of the continent due to the effect of the ocean circulation. Also, the area of maximum downward motion in the continent of the subtropics is shifted westward consistently with the westward shift of the arid zone mentioned before. In the oceanic region of high latitudes, the intensity of upward motion is increased somewhat off the west coast of the continent.

In subsection 8A, it will be demonstrated that the modification of the vertical *P*-velocity described above is closely related to that of precipitation caused by the energy exchange between the ocean and the atmosphere.

E. SURFACE PRESSURE

The latitudinal distributions of zonal mean surface pressure of the joint model and that of the A-model are compared in figure 20. According to this figure, both the subtropical High and the low-pressure belt of the middle-latitude region are less pronounced in the joint model than in the A-model. Also, the polar High is somewhat weaker in the former than in the latter. Since the meridional gradient of surface pressure generally tends to enhance the intensity of meridional cells, these results are consistent with the weakening of meridional cells described in the previous subsection.

In this figure, the observed distributions of annual mean, zonal mean surface pressure in both hemispheres

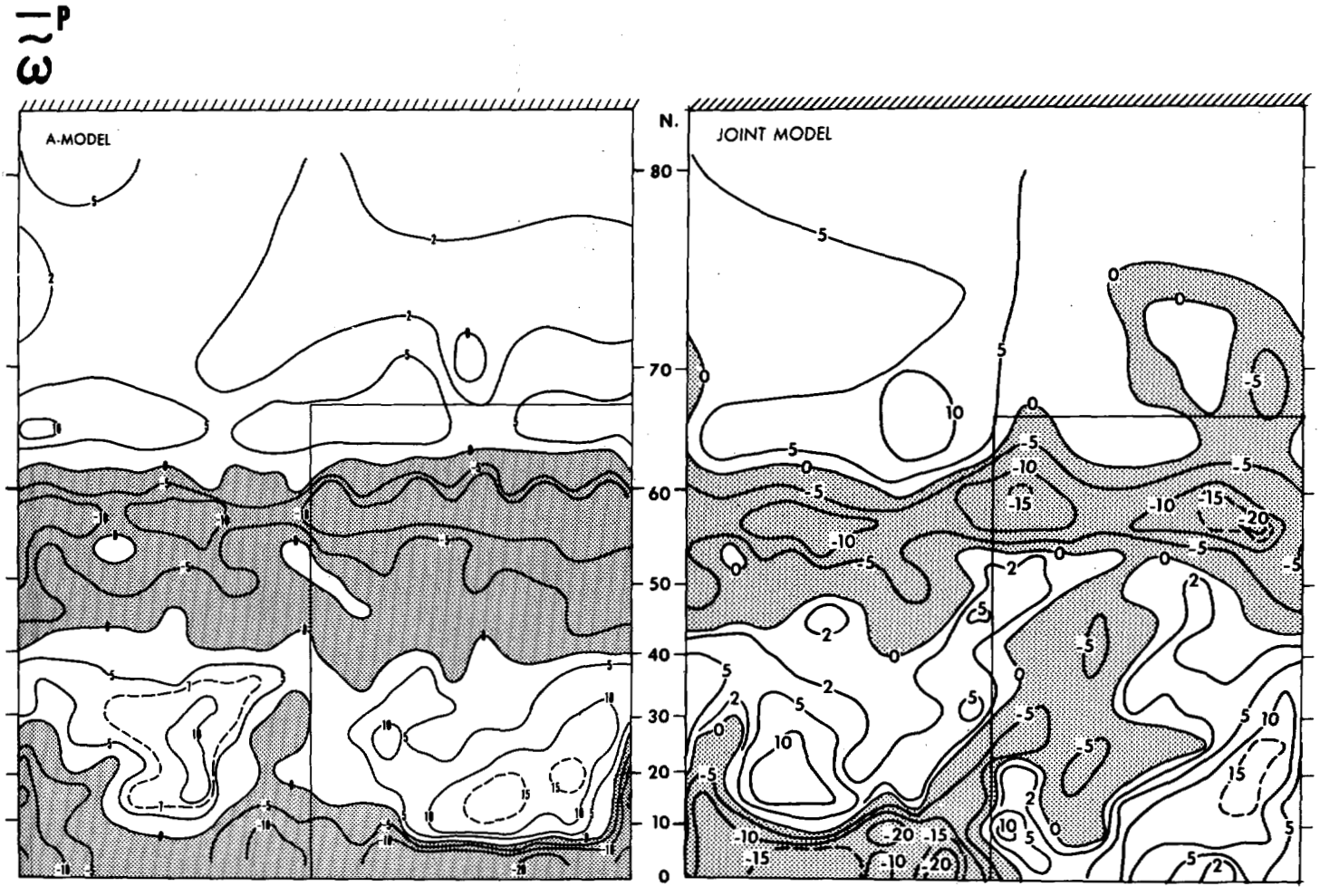

FIGURE 19.—Areal distributions of the vertical mean (mass-weighted) vertical P-velocity (mb day $^{-1}$).

are also plotted for comparison with the model results. The zonal mean pressure of the Northern Hemisphere, however, is so much different from the zonal mean pressure of the Southern Hemisphere that it is almost impossible to evaluate the degree of similarity of the model distributions of pressure to the actual distribution. Nevertheless, it seems to be clear that the polar High appears too pronounced in both models due to the cold pool of air on the snow-covered polar cap.

Figure 21 was constructed to show how the surface pressure of the continent and of the ocean differ from one another. In the subtropics, the surface pressure of the ocean is significantly higher than the surface pressure of the continent, indicating the development of an oceanic anticyclone. As we explained in part I, the temperature of the air on the subtropical desert is much higher than on the subtropical ocean due to insufficient soil moisture in the desert. This difference in temperature causes the difference in surface pressure (through the hydrostatic relationship) and is responsible for the development of this oceanic anticyclone.

In higher latitudes, the surface pressure of the oceanic region is significantly lower than the surface pressure of the continental region due to the warm sea-surface temperature and to the rapid development of cyclone waves off the east coast of the continent, discussed in the next section. In figure 22, showing the areal distribution of the surface pressure of the joint model, the extensive area of low pressure spreads all the way to the coastline of the polar continent, reminding us of the Aleutian Low in the actual atmosphere. The corresponding area of low pressure of the A-model does not extend so far poleward (fig. 9A of part I).

6. EDDY KINETIC ENERGY

In figure 23, the zonal mean eddy kinetic energy at the 500-mb level of the joint model is compared with the zonal mean kinetic energy at the same level of the A-model atmosphere. According to this comparison, the magnitude of the former is significantly smaller than the magnitude of the latter in middle latitudes. The poleward transport of heat by ocean currents reduces the meridional temperature gradient and hence the magnitude of the vertical zonal wind shear. The theory of baroclinic instability indicates that the reduction of vertical wind shear suppresses the development of baroclinic waves in the atmosphere. This is why the magnitude of the eddy kinetic energy of the joint model is smaller than that of the A-model. Figure 24 shows the latitudinal distributions of the conversion of eddy potential energy into eddy kinetic energy caused by transient eddies in both model atmospheres. In middle latitudes, the eddy conversion in

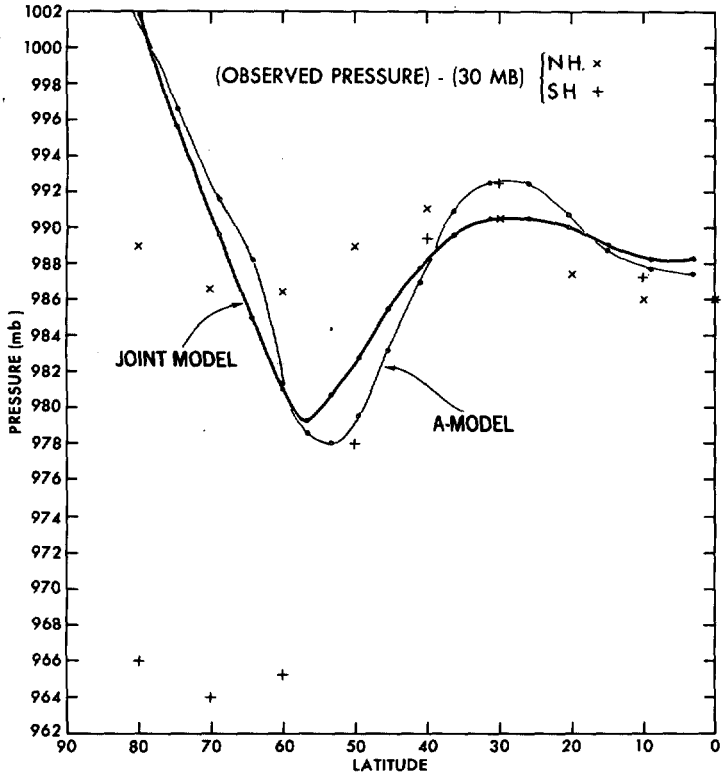

FIGURE 20.—Latitudinal distributions of the zonal mean values of surface pressure; heavy line, the distribution for the joint model; light line, the distribution for the A-model; x, the observed zonal mean value for the Northern Hemisphere and + for the Southern Hemisphere.

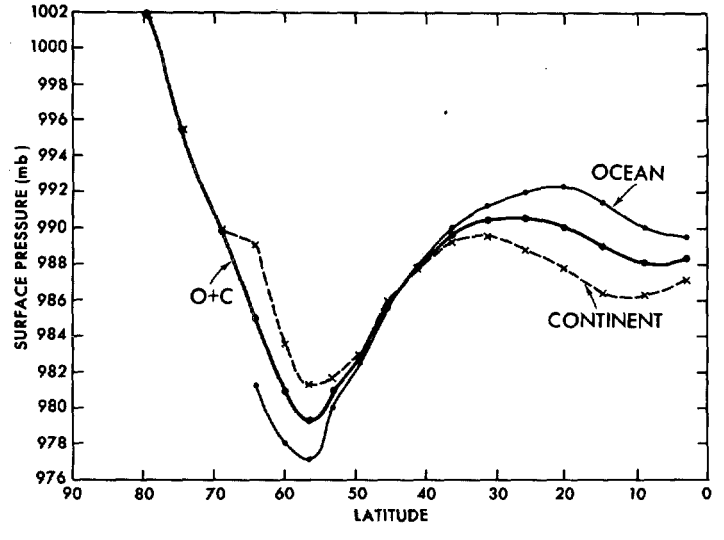

FIGURE 21.—Zonal mean surface pressure on the continent (dashed line); on the ocean (light solid line); and at the earth's surface (average of continental value and oceanic value), heavy solid line.

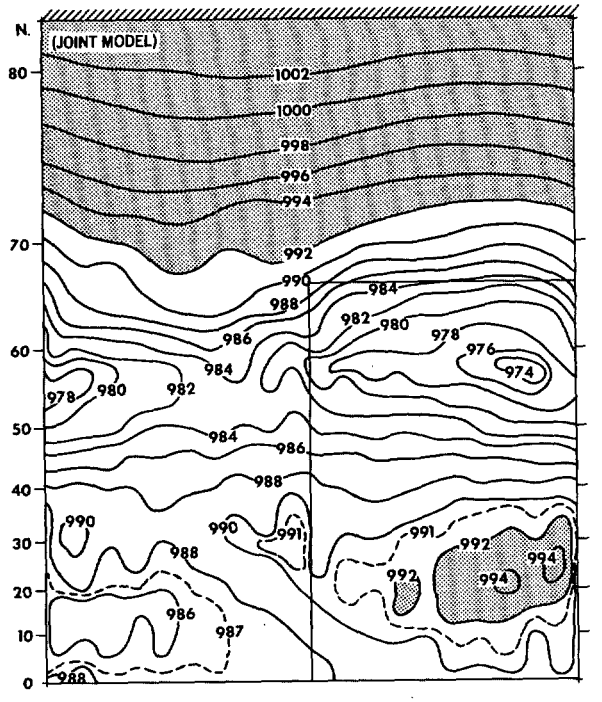

FIGURE 22.—Areal distribution of surface pressure of the joint model atmosphere (millibars).

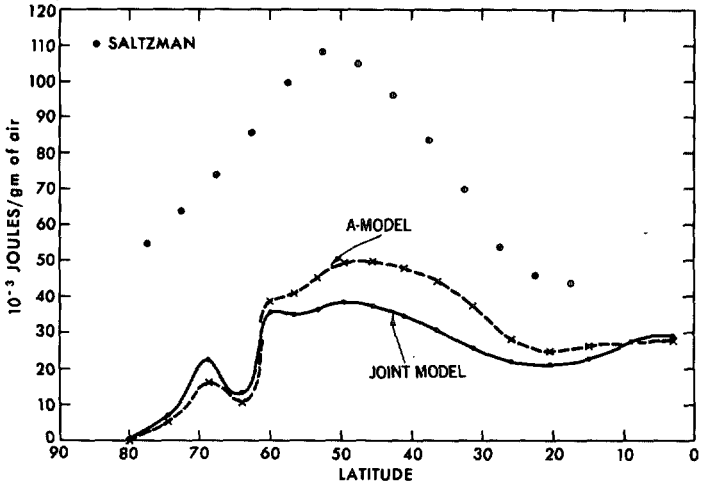

FIGURE 23.—Latitudinal distributions of the zonal mean value of the eddy kinetic energy at the 500-mb level; solid line, distribution of the joint model; dashed line, distribution of the A-model; and the larger dots, annual mean values of eddy kinetic energy in the actual atmosphere (Saltzman, 1962).

the joint model atmosphere is significantly smaller than the eddy conversion in the A-model atmosphere and accounts for the difference of eddy kinetic energy mentioned above.

In order to compare the magnitude of eddy kinetic energy in the model atmospheres with that of the actual atmosphere, the estimates of annual mean values of eddy kinetic energy in the actual atmosphere (Saltzman, 1962) are added to figure 23. According to this comparison, the model atmospheres have much less eddy kinetic energy than the actual atmosphere. The result of more recent numerical experiments conducted at the Geophysical Fluid Dynamics Laboratory of ESSA (Manabe and others, 1970) suggests that the increased resolution for horizontal finite differencing results in the increase of eddy kinetic energy in the model atmosphere. Further study is necessary to clarify the cause of this discrepancy.

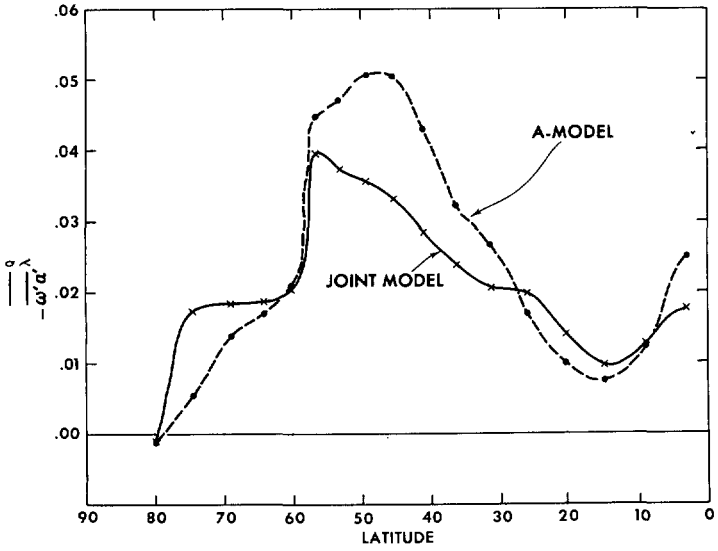

FIGURE 24.—Latitudinal distributions of the zonal mean conversion of potential energy due to transient eddies; units, 10^3 joules cm^{-2} day^{-1}.

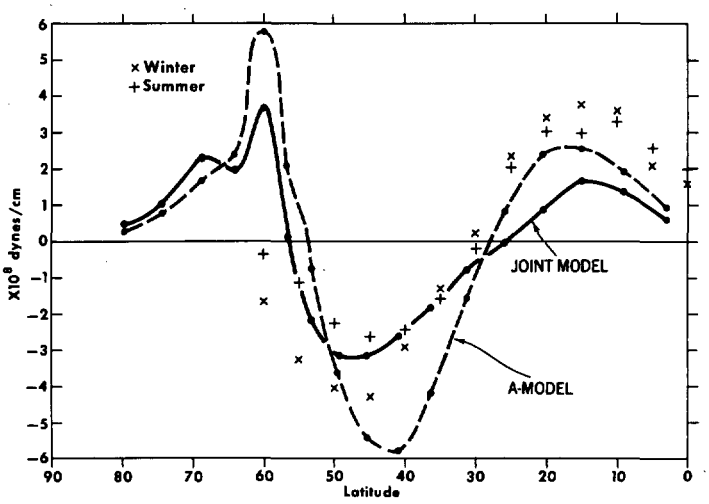

FIGURE 26.—Latitudinal distributions of the zonal mean surface torque. The values of surface torque on the actual ocean surface, estimated by Priestley (1951), are plotted by x's for winter and +'s for summer.

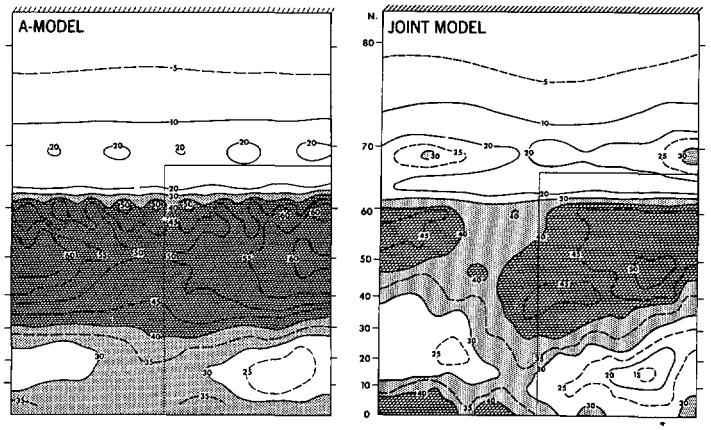

FIGURE 25.—Areal distributions of vertically integrated eddy kinetic energy (units, joules cm^{-2}).

In figure 25, the areal distribution of the vertical mean (mass-weighted) eddy kinetic energy of the joint model is also compared with that of the A-model. One of the interesting features of the distribution of the joint model is that in middle and high latitudes the eddy kinetic energy in the oceanic region is larger than in the continental region. Since this difference is hardly detectable in the A-model distribution, the ocean circulation seems to be mainly responsible for this feature. The large land-sea contrast of temperature along the east coast of the continent in high latitudes, which is chiefly maintained by the oceanic advection of heat, promotes the development of cyclones off the east coast of the continent. It is well known by synoptic meteorologists that cyclone development generally predominates in the vicinity of the Aleutian Archipelago in the Pacific Ocean or in the vicinity of Iceland in the Atlantic Ocean. In short, the behavior of the joint model is in qualitative agreement with the behavior of the actual atmosphere.

It is interesting that the distribution of the eddy kinetic energy of both models shows a weak secondary maximum in the tropical rain belt. The eddy conversion (fig. 24) also has a secondary maximum. As Manabe and Smagorinsky (1967) pointed out, this weak maximum of eddy kinetic energy distribution is maintained by the release of eddy available potential energy generated by the heat of condensation. For the joint model, the tropical maximum is located in the continental Tropics, where the intensity of rainfall is a maximum.

In the model subtropics, the eddy kinetic energy is generally small. However, it is relatively large along the east coast of the continent, where cyclones are generated frequently (see section 8 of part I) and precipitation (fig. 28) is relatively abundant.

7. BUDGET OF ANGULAR MOMENTUM

In order to compare the budget of angular momentum in the two models, the latitudinal distributions of the surface torque are shown in figure 26. In the Tropics and polar regions, surface easterlies predominate and the atmosphere receives the angular momentum from the earth's surface; whereas in middle latitudes, it loses angular momentum to the earth's surface because of the predominance of surface westerlies. In figure 26, the magnitude of the exchange for the joint model is significantly smaller than for the A-model. As we pointed out in subsection 5E, the magnitude of the latitudinal gradient of zonal mean surface pressure of the former is generally smaller than of the latter. Therefore, the surface zonal wind and the surface torque of the joint model are smaller than those of the A-model.

The latitudinal distribution of the imbalance of the angular momentum described above must be compensated for by the meridional transport of the absolute angular momentum. Figure 27 shows the breakdown of poleward

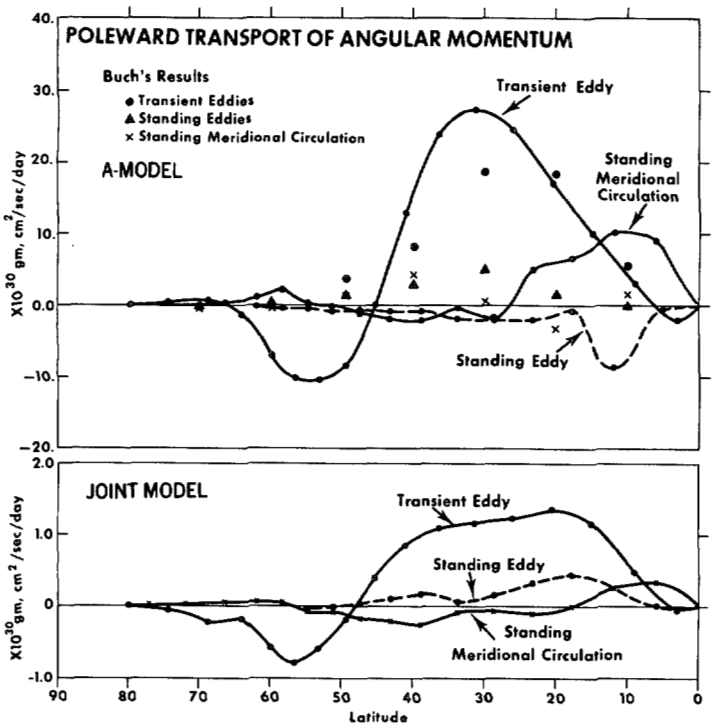

FIGURE 27.—Latitudinal distributions of the poleward transport of angular momentum by meridional circulations, transient eddies, and standing eddies. The transport values in the actual atmosphere, estimated by Buch (1954), are also plotted for comparison.

transport into various components.[4] For comparison, the corresponding distributions for the A-model are also included in figure 27. Comparison shows that the poleward transport of angular momentum by transient eddies in the joint model atmosphere is smaller than that in the A-model atmosphere. Since the magnitude of the momentum exchange of the joint model earth's atmosphere with the surface is less than that of the A-model atmosphere, it is reasonable that the meridional transport of angular momentum by transient eddies should be less in the former than in the latter. This difference in the magnitude of the transport may be partly due to the difference between the magnitudes of the eddy kinetic energy in the two model atmospheres. As mentioned previously, the eddy kinetic energy of the joint model is less than the eddy kinetic energy of the A-model.

8. WATER BALANCE

A. PRECIPITATION

In order to find out how the ocean circulation altered the distribution of precipitation, the areal distribution of precipitation of the joint model is compared with that of the A-model in figure 28. This comparison shows that one of the most drastic differences between the two distribu-

[4] The definitions of transports by transient eddies, standing eddies, and standing meridional circulation were given in subsection 5B of part I.

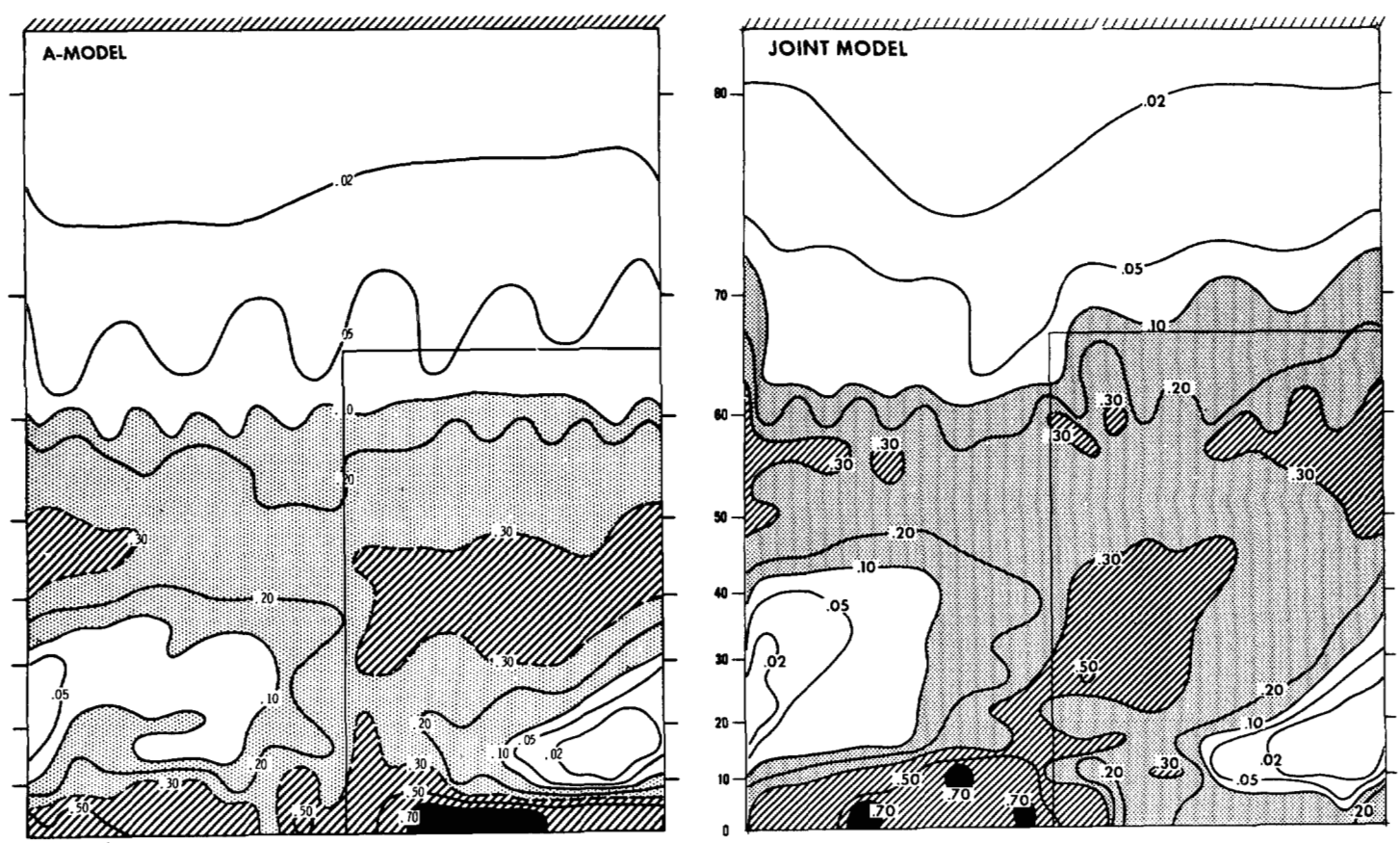

FIGURE 28.—Areal distributions of the rates of precipitation, that is, the sum of the rates of rainfall and snowfall (cm day^{-1}).

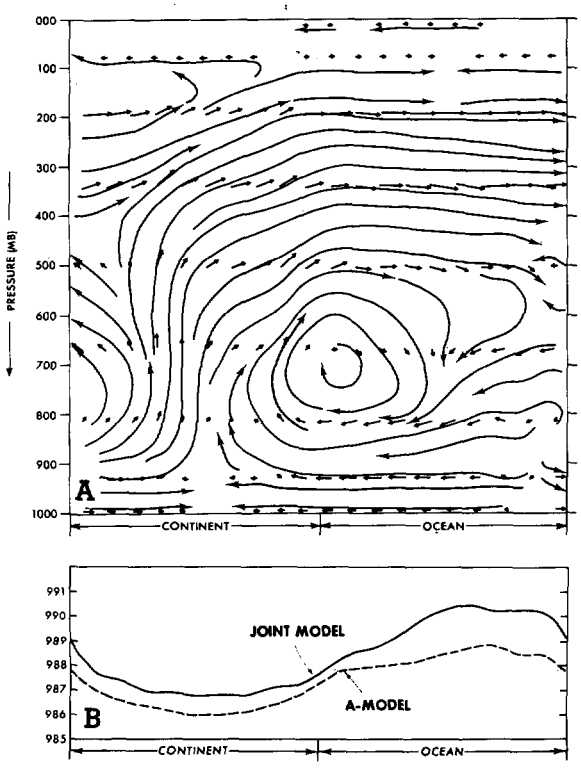

FIGURE 29.—(A) longitude-height cross section of zonal circulation at 3° latitude; thin lines indicate streamlines, and vectors indicate the displacement of the air parcel during two-thirds of the day; (B) the longitudinal distributions of surface pressure at 3° latitude.

tions appears in the Tropics. The intensity of the rainfall in the oceanic region of the Tropics is reduced drastically by the effect of the oceanic circulation. As explained in part III, a belt of relatively cold sea-surface temperature is maintained along the Equator due to the effect of upwelling (see fig. 12 of part II) and is clearly responsible for the suppression of the rainfall in the oceanic region of the Tropics. According to the comparison between the distribution of eddy kinetic energy shown in figure 25 and of precipitation in the Tropics, the area of large eddy kinetic energy tends to be associated with a large rate of precipitation. This tendency is reasonable because most of the tropical rainfall in the model atmosphere is accompanied by tropical cyclones and because the conversion of the eddy available potential energy generated by the heat of condensation is responsible for maintaining the kinetic energy of the model Tropics (Manabe and Smagorinsky, 1967). Since a cold sea-surface temperature tends to prevent moist convection, it may be responsible for the suppression of cyclogenesis and, accordingly, of rainfall in the Tropics. Also, the belt of cold sea-surface temperature tends to lower the rate of evaporation in the Tropics and thus reduce the supply of moisture to the tropical rain belt (subsection 8B).

The drastic decrease of rainfall in the oceanic region is accompanied by an increase in the continental region of the Tropics. In order to clarify the mechanism of these changes, figure 29, showing the distribution of flow in the vertical zonal plane on the joint model Equator, was constructed. Downward motion in this figure appears in the eastern part of the ocean, and intense upward motion prevails in the eastern part of the continent. Such a circulation certainly suppresses the tropical rainfall in the eastern half of the ocean. It also brings abundant moisture from the ocean to the continent and supplies fuel for maintaining the rain belt of the tropical continent. As figure 19 indicates, this type of circulation is absent in the Tropics of the A-model. If one examines the zonal distributions of surface pressure at the Equator of both models, shown in figure 29B, he notices that the oceanic high-pressure region in the eastern part of the tropical ocean is more pronounced for the joint model than for the A-model. This difference in the distribution of the surface pressure may be caused by the cooling due to the belt of cold sea-surface temperature, mentioned above, and may account for the existence of this circulation in the zonal plane on the Equator of the joint model. In other words, the larger zonal gradient of surface pressure at the joint model Equator favors this zonal circulation. A circulation of this kind has been hypothesized by Troup (1965). More recently, Bjerknes (1969) attributed the secular variation of the intensity of the tropical rain belt to the secular variation of this kind of circulation caused by the long-term variation of sea-surface temperature at the Equator. In his paper, Bjerknes called this sort of circulation the "Walker circulation."

The significant increase of intensity of the rainfall in the continental region of the model Tropics, which resulted from this Walker circulation, has a profound effect on the ground hydrology of the model Tropics, discussed in subsection 8C.

In order to compare quantitatively the distribution of the tropical rainfall of the joint model with that of the A-model, the latitudinal distributions of the rate of precipitation in oceanic and continental regions are shown in figure 30. Also, estimates of the actual precipitation are added as references. This figure clearly indicates the sharp reduction of the rate of rainfall in the tropical ocean and the significant increase in the continental region of the Tropics as it is described at the beginning of this subsection. Accordingly, the intensity of the rainfall in the oceanic region of the joint model Tropics is much less than the intensity of the actual rainfall estimated by Budyko (1963). Also, the width of the tropical rain belt over the joint model ocean seems to be too narrow as compared to the width of the actual rain belt. In view of the extreme idealization of land-sea configuration and the lack of seasonal variation in the model, these discrepancies do not necessarily indicate that the effect of ocean circulation is not incorporated properly into the joint model. Rather, this result could be regarded as an excellent manifestation of the suppressing effect of the cold equatorial temperature upon rainfall activity. According to the results of the recent observation of the brightness of the earth from the TIROS satellite compiled by Taylor and Winston (1968) for a period of 1 yr, the tropical rain belt is located on either or both sides of the Equator, depending upon the season, and tends to avoid the Equator. Bjerknes (1969) speculated that this tendency may be due to the equatorial

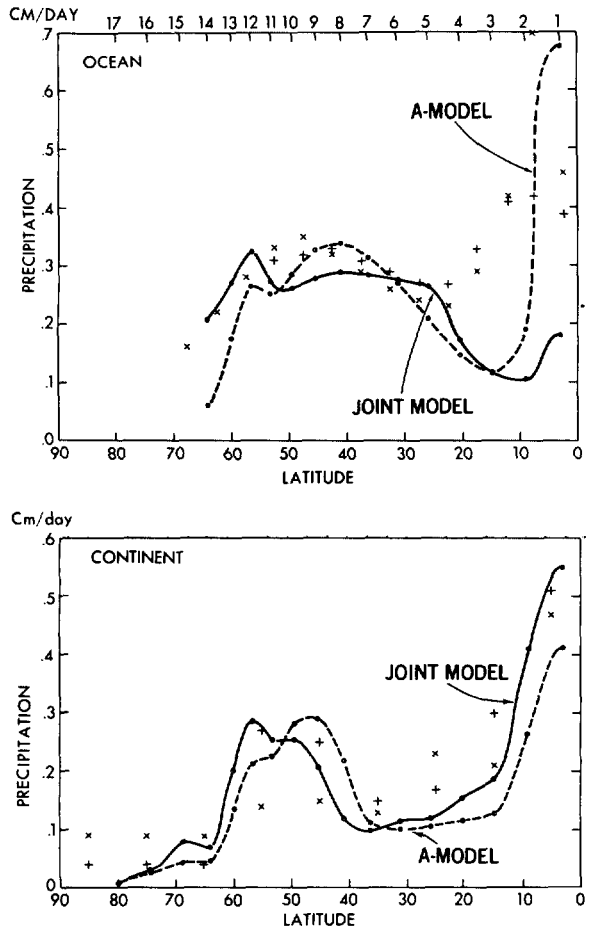

FIGURE 30.—Latitudinal distributions of the zonal mean rate of precipitation of both models in the oceanic region and the continental region. The rates of actual precipitation, estimated by Budyko (1963), are indicated by x's for the Northern Hemisphere and by +'s for the Southern Hemisphere.

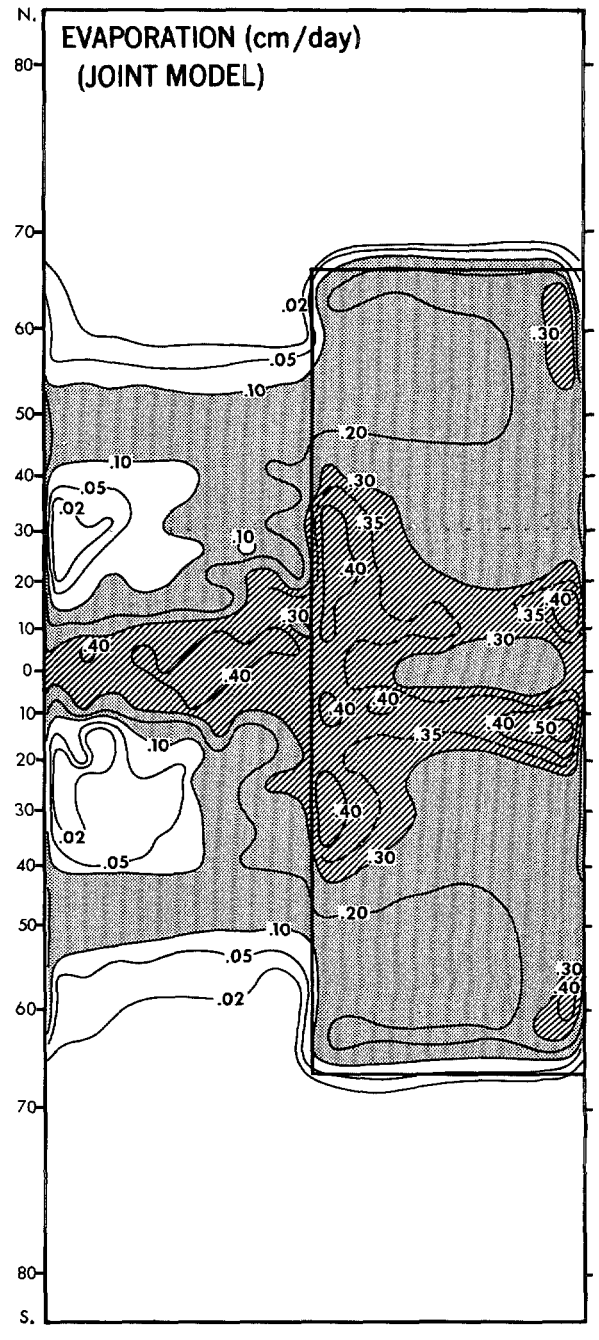

FIGURE 31.—Areal distribution of the rate of evaporation from the earth's surface of the joint model.

belt of cold sea-surface temperature mentioned above. The present result seems to substantiate his speculation. In fact, the preliminary results Wetherald and Manabe (1969) from the time integration of the joint model with the seasonal variation of solar insolation shows the tendency of the tropical rain belt to appear on either side of the Equator, depending upon the angle of the sun, and to avoid the Equator in agreement with the observed features. Also, their results indicate that the lack of seasonal variation of the declination angle of the sun in the present model is responsible for the narrowness of the tropical rain belt mentioned above.

In the subtropics, precipitation along the east coast of the continent significantly increases because of the ocean current effect (fig. 28). As explained in part I, the rate of precipitation in this region is larger than the surrounding region of the subtropics, even without the effect of the ocean current. The heating and moistening of the air by the warm water brought by the subtropical gyre further enhances the precipitation activity in the region. Owing to this modification, the arid region of the subtropical desert is more or less limited to the western half of the continent. This westward concentration of the arid region is evident in the distribution of the temperature of the soil surface and the relative humidity of the lowest model level, shown in figures 12 and 15, respectively. It is noteworthy that the boundary of the arid zone shifts slightly poleward.

According to figure 29 or 31, the rain belt in middle latitudes shifts poleward due to the effect of ocean currents. Particularly, the area of precipitation maximum on and off the west coast of the continent shifts from 45° to 55° latitude. Off the west coast of the continent, the subarctic gyre brings the relatively warm water to higher latitudes, increases the rates of evaporation and of sensible heat flux there, and is responsible for the poleward shift of the rainy area mentioned above.

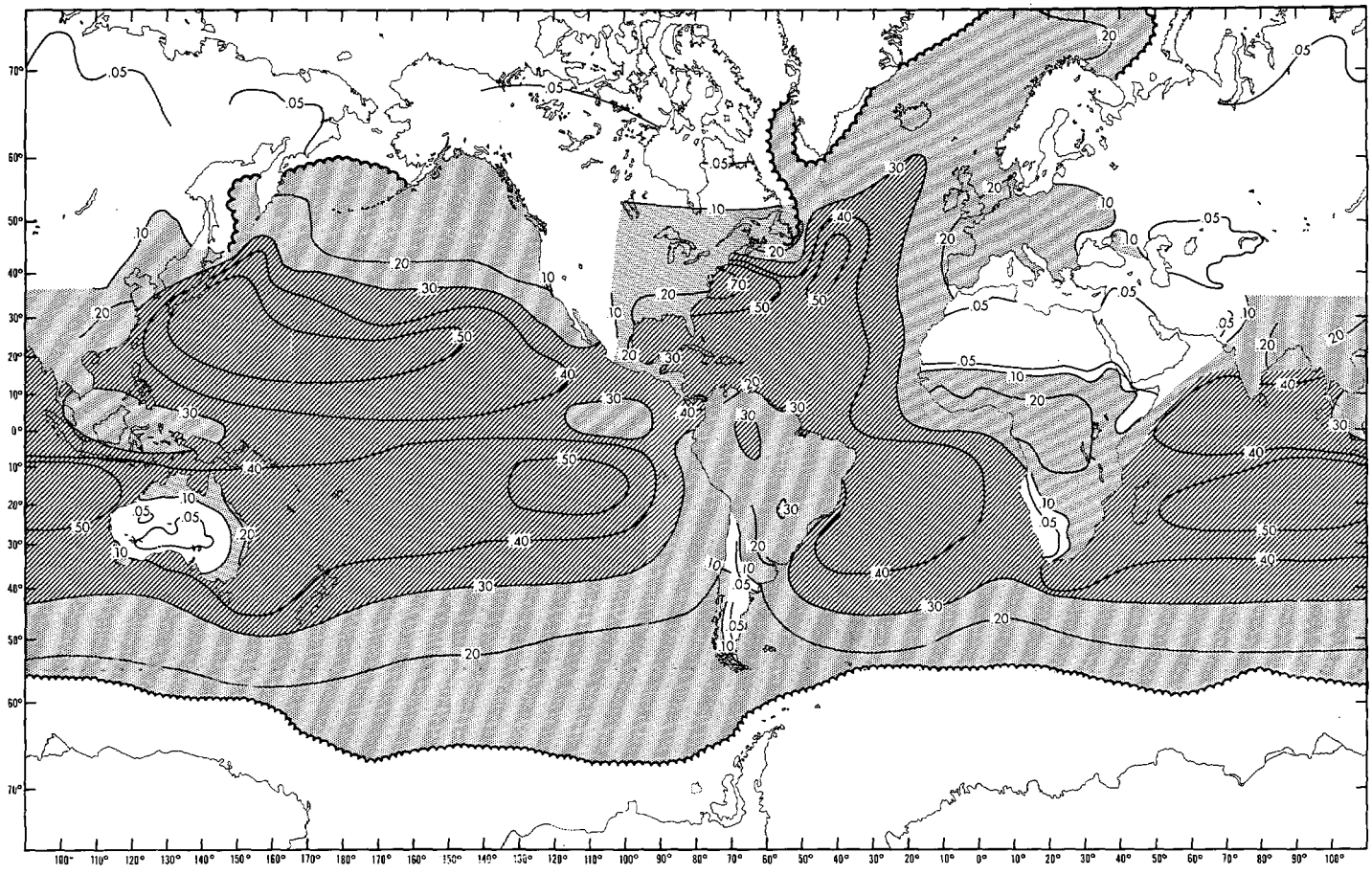

FIGURE 32.—Areal distribution of the rate of evaporation from the actual earth's surface as estimated by Budyko (1963). Units, cm day^{-1}.

B. EVAPORATION

The areal distribution of the rate of evaporation of the joint model is shown in figure 31. In the oceanic region of the joint model Tropics, there is an area of minimum evaporation rate along the Equator. Such a distinct minimum area does not exist in the Tropics of the A-model (fig. 20 of part I). The upwelling of cold water along the Equator, mentioned in the previous sections, reduces the rate of evaporation and is responsible for this minimum area and for the reduction of rainfall amount there. In the continental region of the Tropics, the rate of evaporation, however, is a maximum because the soil is relatively wet due to the tropical rain belt.

In the subtropic and the middle latitudes, the rate of evaporation is very large along the western boundary of the joint model ocean. Such a local belt of maximum evaporation is hardly evident in the oceanic region of the A-model. Accordingly, the longitudinal variation of the rate of evaporation from the joint model ocean in temperate latitudes is much larger than that of the A-model. The advection of heat by the subtropical gyre seems to be responsible for such a variation of evporation rate.

In higher latitudes around 60° to 70°, there is a large land-sea contrast of the rate of evaporation partly because of the large contrast between the albedo of the oceanic region and of the snow-covered continent. A similar contrast is evident in the distribution of the evaporation rate of the A-model shown in figure 20 of part I. The rate of evaporation in the polar boundary of the oceanic region of the joint model, however, is much larger than that of the A-model due to the effect of heat advection by ocean currents. In general, the qualitative features of the distribution of evaporation rate described above are also evident in the distribution obtained by Budyko (1963) and shown in figure 32.

In order to summarize the results of subsections A and B, the latitudinal distribution of the zonal mean rate of the evaporation is compared with that of precipitation in the left-hand part of figure 33. In the right-hand part, the corresponding quantities estimated by Budyko (1963, 1956) are shown for comparison. Although there are many common features between the observed and the computed distributions, as we have pointed out, there is one important difference. The evaporation over the tropical ocean of the joint model is significantly larger than precipitation, in disagreement with the results of Budyko. This previously discussed discrepancy is mainly due to the efficient suppression by the upwelling of cold water along the Equator.

C. RUNOFF

As explained in part I, the computation of runoff is based upon the budget of soil moisture. If the water supply due to the rainfall and snow melt tends to exceed the loss of water due to evaporation, runoff can take place. In figure 34, the areal distributions of runoff of both the A-model and the joint model are shown. This

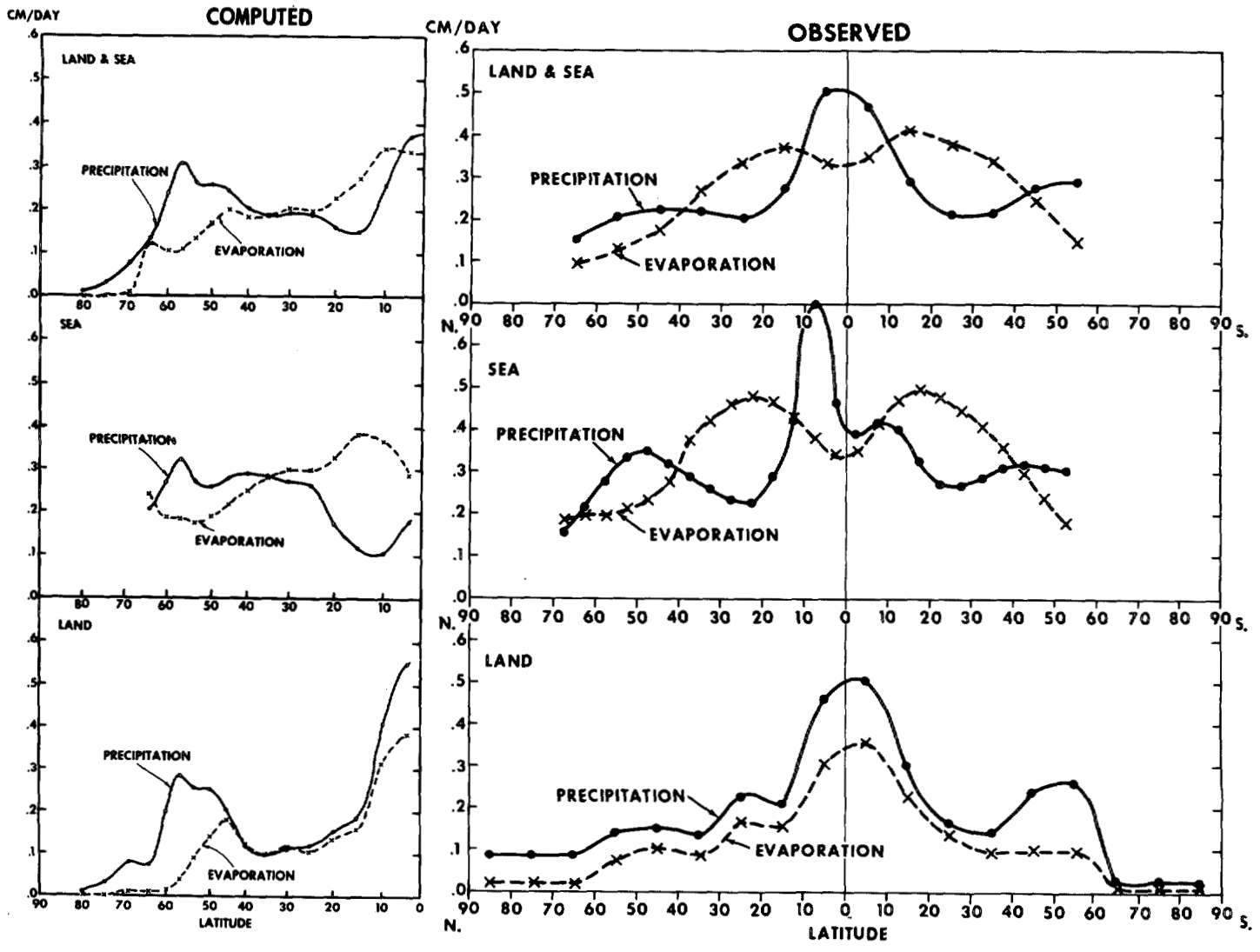

FIGURE 33.—Latitudinal distributions of the zonal mean rates of precipitation (solid lines) and evaporation (dashed lines); left side, the distribution of the joint model; right side, the distribution estimated by Budyko (1963).

comparison shows that the rate of runoff of the joint model is much larger than the rate of runoff of the A-model in the Tropics and the eastern part of the subtropical region of the continent. The increase of the rainfall in these areas due to the effect of the ocean circulation is responsible for this difference. In middle latitudes, an almost zonal belt of runoff is evident in both models. The belt of the joint model, however, extends farther poleward than the belt of the A-model. Again, this difference is consistent with the difference in the distribution of precipitation. As discussed in subsection 8A, the rain belt of middle latitudes extends poleward due to the effect of the ocean circulation.

The latitudinal distribution of the zonal mean excess of precipitation (rainfall plus snowfall) over evaporation, on the continent, for both models is shown in figure 35. In the quasi-steady state, this excess should cause either runoff or iceberg formation depending upon the phase state of water. The zonal mean rates of runoff at the actual earth's surface, obtained by Lvovitch and Ovtchinnikov (1964), are also plotted in figure 35 for comparison. In the Tropics, the amount of runoff from the continent compares well with that obtained by Lvovitch and Ovtchinnikov. The secondary maximum appearing in middle latitudes of the joint model is missing in the distribution of Lvovitch and Ovtchinnikov for the Northern Hemisphere, but is evident in their values for the Southern Hemisphere. It is probable that the large longitudinal dimension of the Eurasian Continent makes it difficult to supply moisture to the inland area and is responsible for reducing the runoff per unit area in middle latitudes of the Northern Hemisphere. In view of the fact that the longitudinal dimension of the continent of the joint model is smaller than that of the Eurasian Continent in the Northern Hemisphere but is similar to that of the continents in the Southern Hemisphere, this distribution of the joint model may be reasonable.

D. SOIL MOISTURE

Owing mainly to the difference in the distribution of precipitation, the areal distribution of soil moisture of the joint model is significantly different from that of the A-model. Figure 35 shows the comparison between the two. In this figure, the area of low soil moisture in the subtropical region of the continent is more or less limited to the western

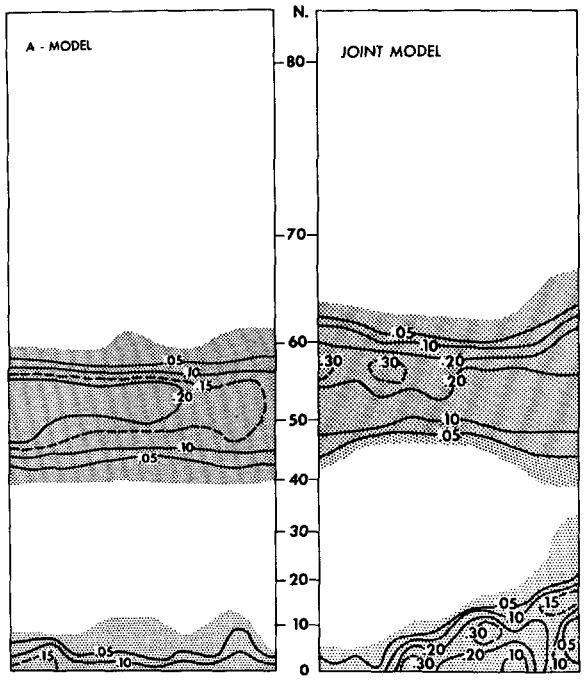

FIGURE 34.—Areal distributions of runoff (cm day^{-1}) in the continental region. The effect of iceberg formation is not included.

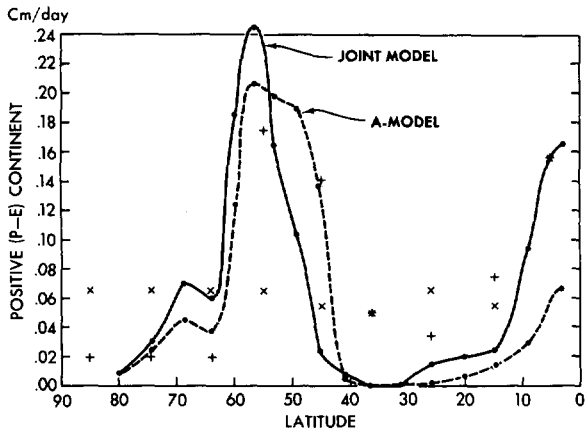

FIGURE 35.—Latitudinal distributions of excesses of zonal mean precipitation over evaporation on the continent. The distributions of zonal mean runoff on the actual continent, obtained by Lvovitch and Ovtchinnikov (1964) are indicated by x's for the Northern Hemisphere and +'s for the Southern Hemisphere.

half of the continent for the joint model; whereas, it occupies part of the eastern half for the A-model. Similar differences were evident in the distributions of relative humidity and surface temperature shown in figures 15 and 12. The increase of rainfall in the eastern half of the subtropical region of the continent, caused by the effect of the ocean circulation, is responsible for this difference. Figure 36 also indicates that the desert area of the joint model extends farther poleward than the desert area of the A-model. This extension may be related to the poleward shift of the rain belt in the middle latitude due to the effect of the ocean currents (subsection 8A). In the Tropics, the

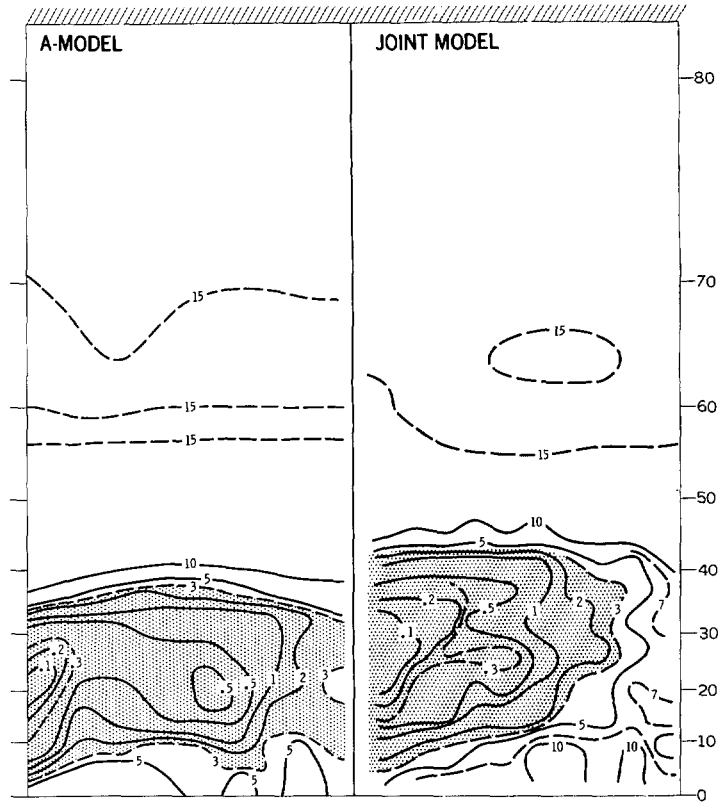

FIGURE 36.—Areal distributions of soil moisture (centimeters) in the continental region.

soil moisture of the joint model is significantly larger than the soil moisture of the A-model. As described in subsection 8A, the intensity of the tropical rainfall over the continent increases markedly due to the effect of the ocean currents. This increase is responsible for the difference in the amount of soil moisture mentioned above.

E. SNOW BUDGET

One of the most important hydrologic factors affecting the climate is snow cover, with its large albedo for solar radiation. Figure 37 shows the latitudinal distributions of the various components affecting the snow budget on the continent. The snow budget of the joint model is shown in the upper part of the figure and the snow budget of the A-model in the lower part. According to this figure, snow accumulates poleward of 58° latitude in the joint model, whereas it accumulates poleward of 53° in the A-model. In other words, the equatorward boundary of snow cover shifts poleward due to the effect of the ocean circulation. Also, the maximum rate of accumulation in the joint model is much less than in the A-model. These results indicate the existence of the following positive feedback mechanism, which has been suggested by various authors (Opik, 1953, for example). The poleward advection of heat energy by ocean currents raises the air temperature at higher latitudes and, accordingly, increases the rate of snow melt and the ratio of rainfall to snowfall. The resulting decrease of snow cover decreases the albedo of the earth and raises further the temperature of the earth's surface.

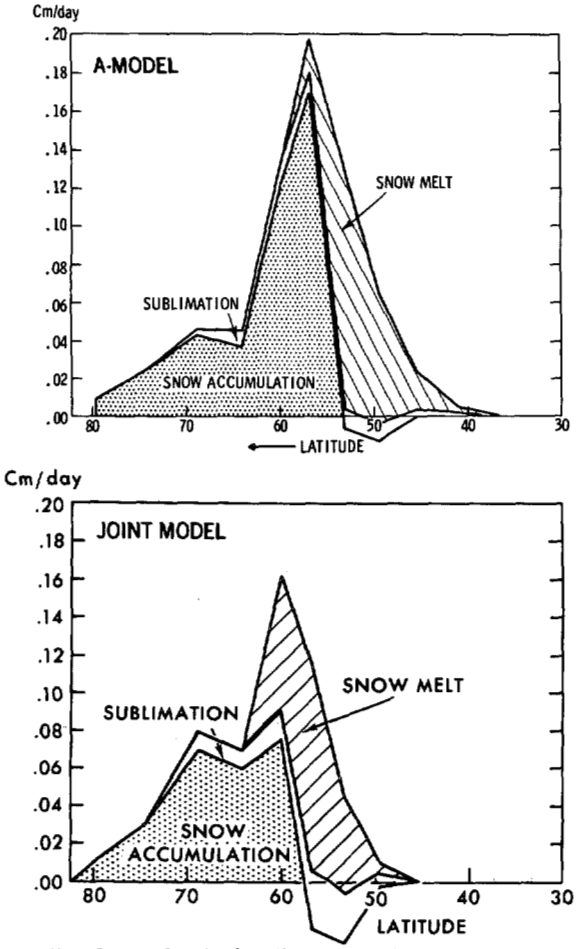

FIGURE 37.—Latitudinal distributions of zonal mean rates of various snow budget components (snowfall, snow melt, and sublimation) on the continental surface.

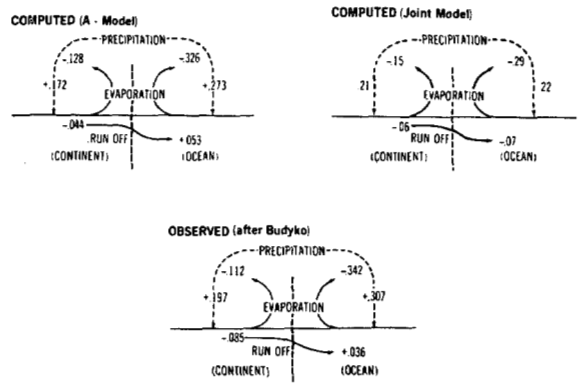

FIGURE 38.—Areal mean rates of water balance components on the continent and ocean, that is, evaporation and sublimation, rainfall and snowfall, and runoff and iceberg formation in units of cm day^{-1}. Upper left, rates for the A-model; upper right, rates for the joint model; and lower part, rates for the actual earth's surface estimated by Budyko (1963).

Despite the warming effect of the ocean circulation on the climate, which we have described so far, snow nevertheless accumulates poleward of 58° latitude. In the long run, such an accumulation of snow cover would result in a glacial period. Unpublished results (Wetherald and Manabe, 1969) from a recent numerical experiment indicate this excessive accumulation of snow cover can be prevented by introducing the effect of seasonal variation of insolation.

F. WATER BALANCE DIAGRAM

In order to find out how the water balance of the continent and of the ocean as a whole is affected by the ocean circulation, diagrams of the water balance are constructed for both models and are shown in figure 38. From Budyko (1963), a similar diagram can be constructed for the actual atmosphere; for comparison, this is included in figure 38. In this figure, the rainfall on the ocean decreased by about 20 percent, whereas the rainfall on the continent increased by about 25 percent, due to the effect of the ocean circulation. The main reasons for these changes are the drastic weakening of the tropical rain belt on the ocean due to the effect of cold sea-surface temperatures and the resulting intensification of the rain belt in the continental region of the Tropics. These changes in the distribution of tropical rain, in turn, increase the runoff from the Tropics and increase the total runoff from continent to ocean, as figure 38 indicates.

In general, the intensity of the hydrologic cycle in both model atmospheres seems to be significantly (20 percent) less than in the actual atmosphere. The areal mean rate of precipitation is about 0.22 cm day^{-1} for both the joint model and the A-model. On the other hand, the rate estimated by Budyko (1963) is 0.27 cm day^{-1}. One of the reasons for this discrepancy may be the difference in the relative size of the ocean and continent. (Ocean occupies slightly less than half of the whole area of the models; whereas, it occupies approximately two-thirds of the surface of the actual earth.) A numerical integration with realistic topography may be necessary to assess this possibility.

9. HEAT BALANCE

A. HEAT BALANCE OF THE EARTH-ATMOSPHERE SYSTEM

The latitudinal distribution of net radiation at the top of the atmosphere determines the magnitude of the poleward transport of heat energy by the joint ocean-atmosphere system and is one of the most fundamental quantities controlling the general circulation of the atmosphere and the ocean. In figure 39, the distributions of net solar radiation (positive downward) and of net long-wave radiation (positive upward) at the top of the atmosphere are shown as functions of latitude. The difference between these two radiation fluxes represents the radiative imbalance of the joint system and is responsible for the meridional transport of energy. For comparison, the radiative fluxes of the A-model are also indicated in the figure by a thin line. This comparison shows that the net solar radiation in the joint model is slightly more than in the A-model near 55° latitude due to the poleward retreat of snow cover and that the latitudinal gradient of net long-wave radiation in the joint model is slightly less than in the A-model. As a whole, the ocean circulation increases the latitudinal contrast of the radiation imbalance only slightly because

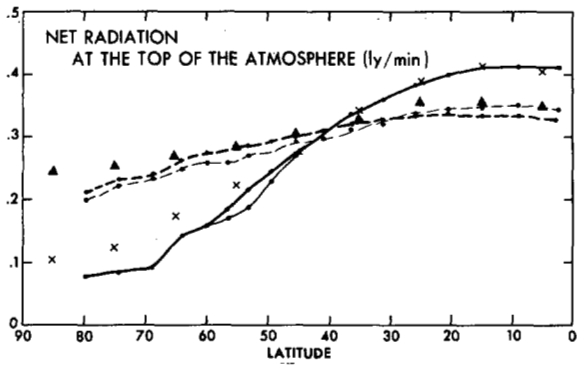

FIGURE 39.—Latitudinal distributions of zonal mean rates of net downward solar radiation (solid lines) and of net upward long-wave radiation (dashed lines) at the top of the atmosphere. Heavy lines indicate the distributions for the joint model and light lines for the A-model. The corresponding quantities by London (1957) for the actual atmosphere are also plotted, using x's and solid triangles for the estimated values of net downward solar radiation and those of net upward long-wave radiation, respectively.

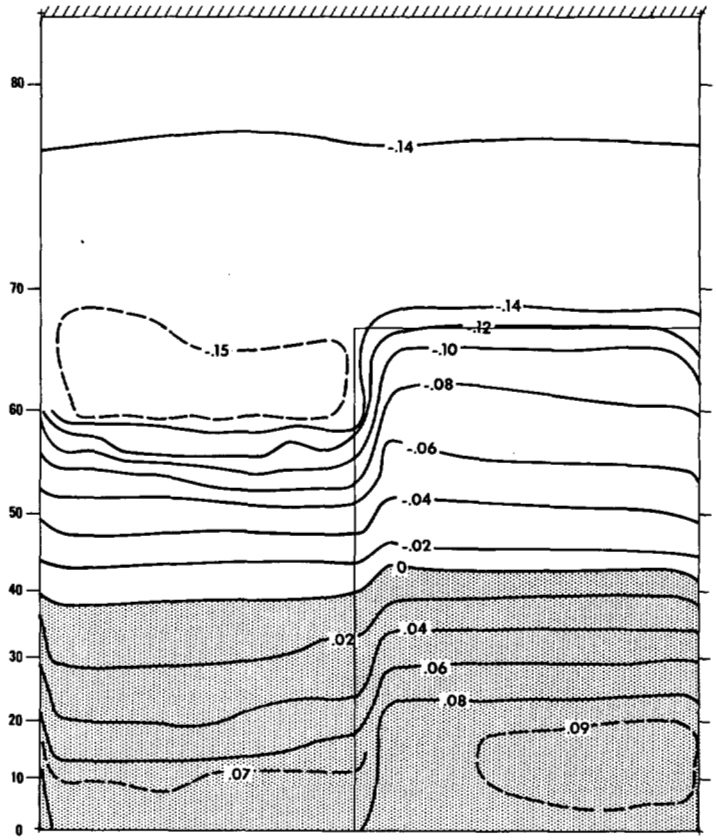

FIGURE 40.—Areal distribution of the flux of net downward radiation (net downward solar radiation minus net upward long-wave radiation) at the top of the joint model atmosphere in units of ly min^{-1}.

it mainly influences the temperature of the lower troposphere (fig. 10). Therefore, its effect on the outgoing radiation at the top of the model atmosphere is minimized by the absorbers in the upper half of the atmosphere.

The areal distribution of net radiation, which is the difference between the net downward solar radiation and the net upward long-wave radiation at the top of the atmosphere, is shown in figure 40. This distribution is very similar to the corresponding distribution of the A-model (fig. 36A of part I). In high latitudes, the land-sea contrast of net radiation in the joint model, however, is less pronounced than in the A-model due to poleward retreat of the snow cover.

B. HEAT BALANCE OF THE EARTH'S SURFACE

Heat balance of the oceanic surface—The heat balance components at the ocean surface are the sensible heat flux, the latent heat flux, and the net radiation flux, the latter representing the difference between net downward solar radiation and net upward long-wave radiation. In addition to these components, there is the heat exchange with the interior of the ocean, which is mostly compensated by the poleward heat transport by ocean currents. In figure 41A, the latitudinal distributions of the zonal mean values of these components at the ocean surface are shown. The thick solid lines and thin solid lines indicate the distribution of the joint model and of the A-model.

According to this figure, the heating of the ocean surface due to net radiation is mostly compensated by the cooling due to evaporation, which is much larger than the cooling due to the flux of sensible heat. The relative importance of the sensible heat, however, increases with increasing latitude because of the decrease of the rate of evaporation with increasing latitude. Figure 41 also indicates that the latitudinal variations of net radiation and of sensible heat tend to increase the meridional gradient of temperature, whereas that of the latent heat flux tends to diminish it. The imbalance among these factors is compensated by the heat flow from the ocean. These features of the distributions are in excellent qualitative agreement with those of the actual ocean surface obtained by Budyko (1963) and shown in figure 41B.

There are, however, some quantitative differences. For example, the magnitudes of sensible heat and latent heat flux around the polar boundary of the joint model ocean are much larger than those over the actual ocean in high latitudes. On the other hand, the heat flow from the interior to the surface along the polar boundary of the joint model ocean is much larger than the heat flow estimated by Budyko (1963) and compensates for the large heat loss due to the large turbulent flux of energy mentioned above. The large air-sea temperature difference around the polar boundary of the model ocean is responsible for these results. In the subtropics, the upward flux of latent energy from the joint model ocean is significantly less than from the actual ocean estimated by Budyko (1963). The cause of this discrepancy is not obvious.

In order to identify the effect of ocean circulation on the heat balance of the ocean, the latitudinal distributions of heat balance components of the A-model are added to figure 41 and are compared with those of the joint model. In high latitudes, the heat flow from the ocean is positive and raises the sea-surface temperature,

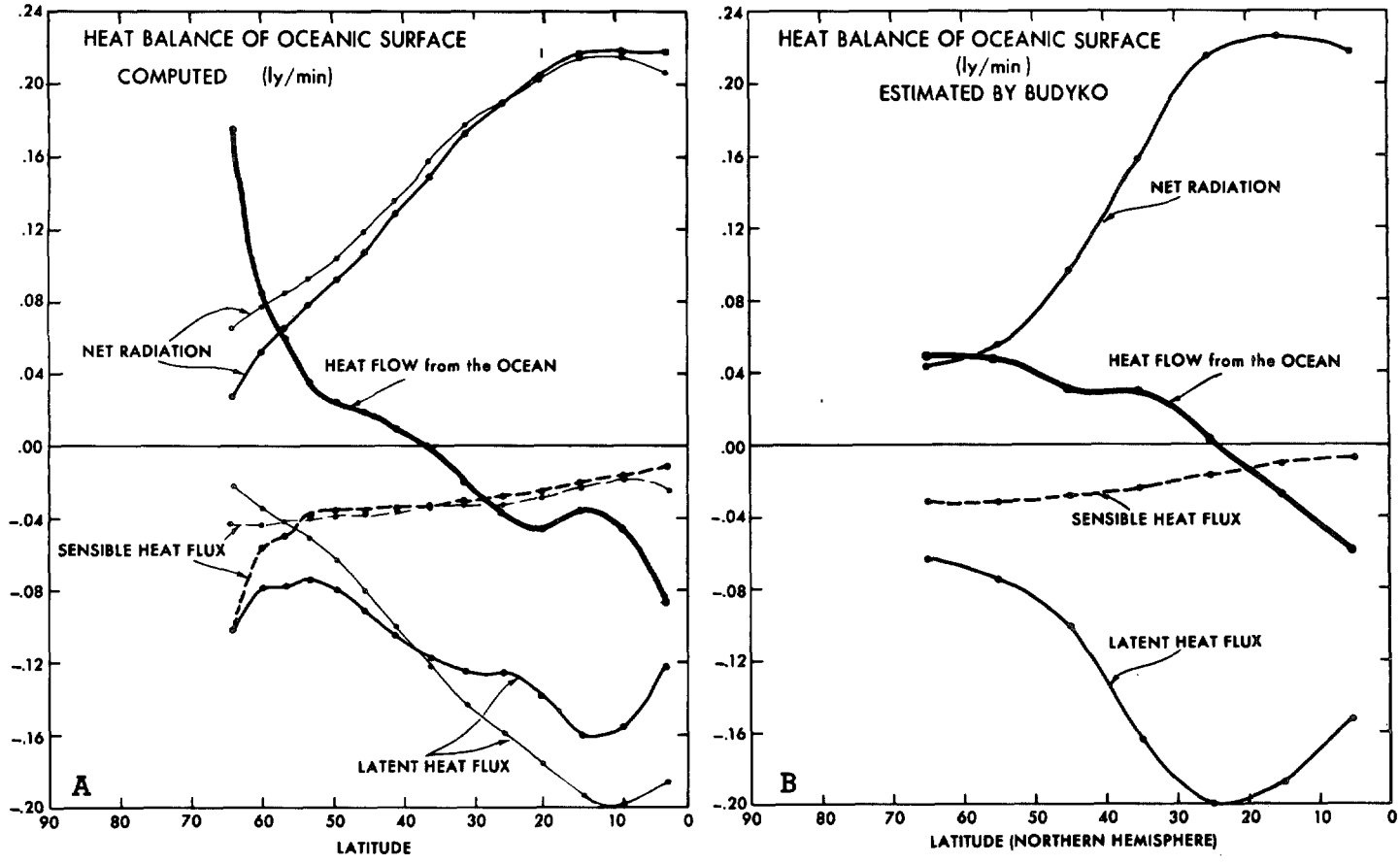

FIGURE 41.—Zonal mean rates of heating of the ocean surface due to net radiation, latent heat flux, sensible heat flux, and heat flow from the interior to the surface of the model. (A) the distributions of the joint model ocean and the A-model ocean are shown by heavy lines and light lines, respectively (note that the heat flow from the ocean is zero for the A-model); (B) distributions for the actual ocean surface as estimated by Budyko (1963).

as figure 12 indicates. Accordingly, both sensible and latent heat flux increase, and net radiation decreases significantly. In low latitudes, the heat flow is negative and lowers the sea-surface temperature. The resulting decrease in the magnitude of latent heat flux is evident in figure 41. In other words, the decrease of the latitudinal gradient of the surface temperature of the model ocean due to the oceanic heat flow increases the latitudinal variation of heat gain by net radiation and decreases that of heat loss by evaporation.

The areal mean value of the heat flow shown in figure 41 is about -0.01 ly min^{-1}, indicating the existence of a net downward flow of heat from the surface to the interior of the ocean. Such a heat flow should cause a slow rise of the ocean mean temperature with time. The existence of a net downward flow of heat at the ocean surface is one of the manifestations of the fact that the thermal structure of the deeper ocean is still far from equilibrium, as described in part III. Though the magnitude of the net flow is not large, it is probable that it lowers the mean temperature of the model atmosphere, reduces the rate of evaporation from the ocean surface, and lowers the general level of the hydrologic cycle in the model atmosphere. Further study is necessary for the quantitative assessment of the effect of this downward heat flow.

The areal distribution of the heat flow from the interior to the surface of the ocean is shown in figure 42. In general, the heat supply to the surface of the model ocean is negative (downward) in low latitudes and is positive (upward) in high latitudes, as indicated above. The poleward transport of heat by ocean currents is obviously responsible for this latitudinal distribution. Near 35° latitude, an area of relatively large heat supply exists along the east coast of the continent due to the poleward advection of the warm water by the subarctic gyre. Poleward of 60°, an area of intense heat supply is evident off the west coast of the continent. This area coincides with the area of warm advection by the subarctic gyre. Another interesting feature of the distribution of the heat flow is the belt of relatively large negative (downward) heat flow around the Equator. As discussed, the upwelling of cold water at the Equator increases the magnitude of the heat loss there.

The distribution of heat flow at the ocean surface described above seems to be closely connected with the way in which the rate of precipitation is modified by the effect of ocean circulation. For example, the equatorial belt of downward heat flow mentioned above corresponds with that of the suppression of precipitation described in subsection 8A. Also, the area of maximum upward heat flow is located in the area where the intensity of precipitation significantly increases due to the effect of ocean circula-

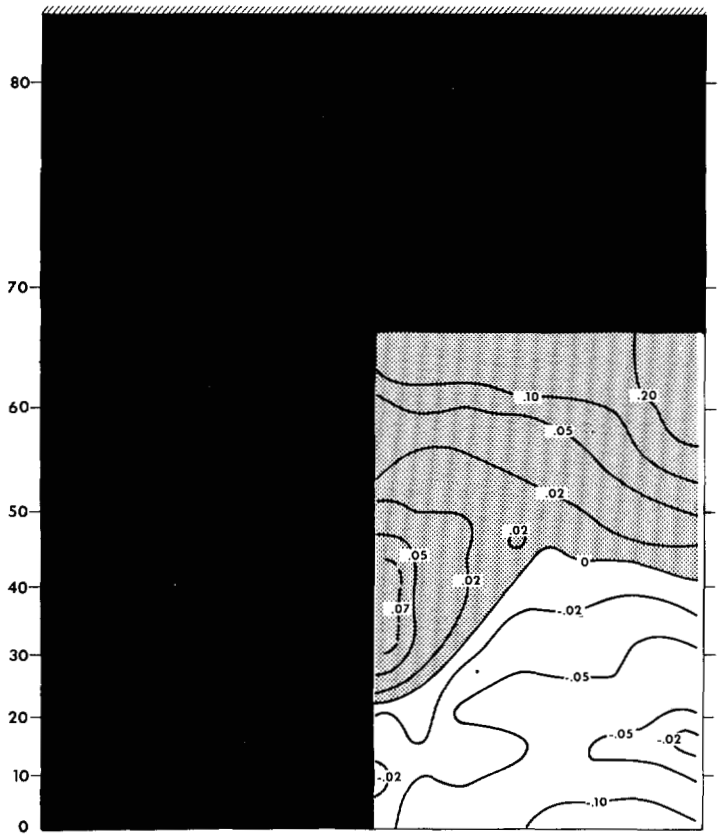

FIGURE 42.—Areal distribution of the heat flow from the interior to the surface of the joint model ocean in units of ly min^{-1}.

tion, that is, along the east coast of the continent and off the west coast of the high-latitude region of the continent.

The distribution of heat flow from the interior to the surface of the ocean, described above, also corresponds well with the way in which the turbulent fluxes of sensible and latent heat from the ocean surface to the atmosphere are modified by the ocean circulation. The areal distributions of these fluxes of the joint model are shown in figure 43, and those of the A-model are shown in figure 47 of part I. Along the east coast of the continent, the turbulent fluxes of sensible and latent heat at the joint model ocean surface are significantly larger than those at the A-model ocean surface. Also, a distinct maximum in both of these fluxes is evident off the west coast of the continent of the joint model near 60° latitude. The area of large turbulent fluxes described here coincides closely with the area of large heat flow from the interior to the surface of the ocean. At the Equator of both models, a belt of minimum latent heat flux is evident. The joint model, however, has a more distinct minimum than the A-model. Again, the belt coincides with the equatorial belt of negative heat flow mentioned above. In short, the heat advection by ocean currents strongly affects the distribution of the turbulent fluxes of sensible and latent heat, which in turn influences the intensity of precipitation. It must also be pointed out that, in general, the areal distribution of the sensible and latent heat fluxes over the ocean is modified by the effect of ocean current in

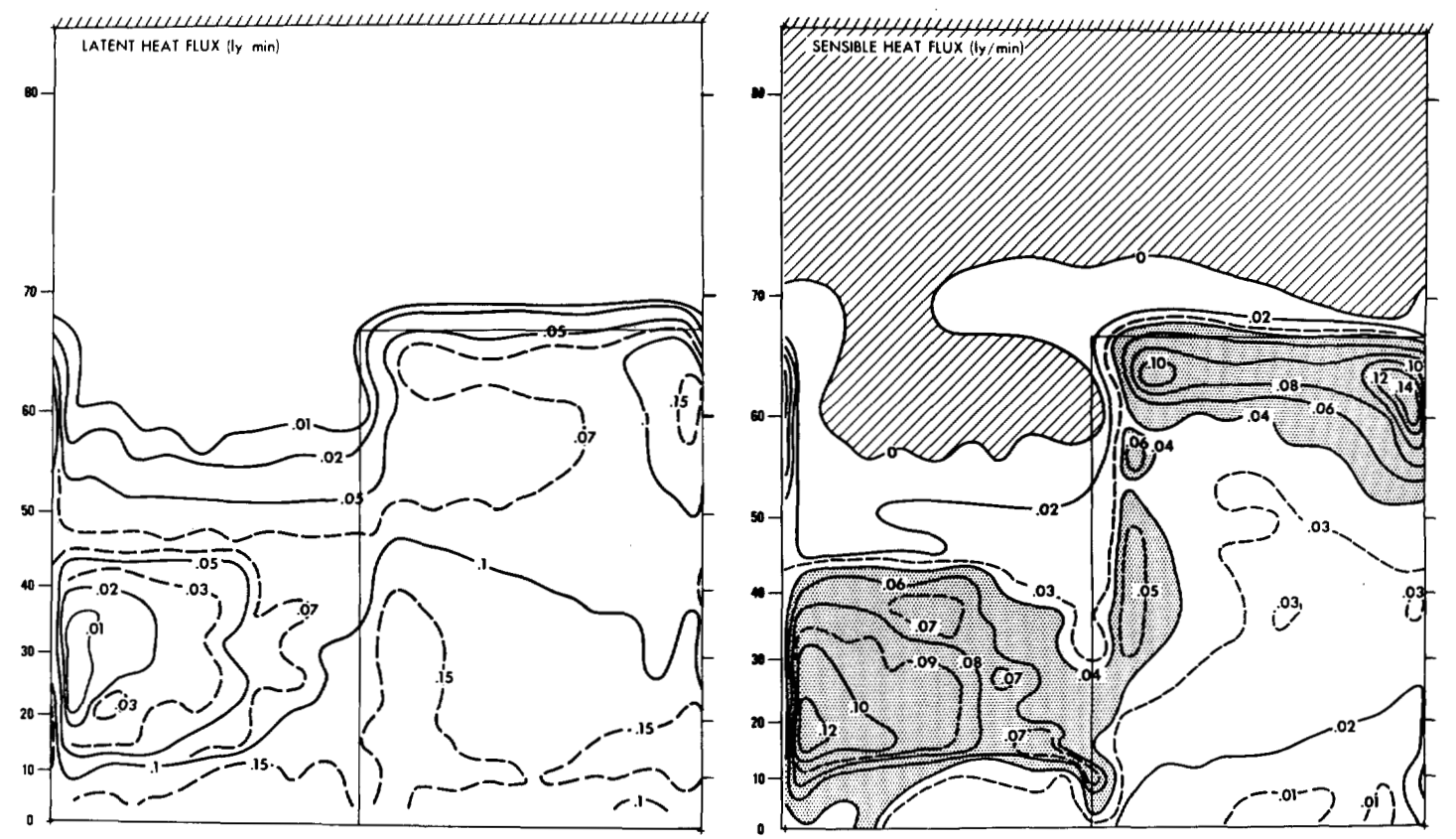

FIGURE 43.—Areal distributions of upward flux of latent and sensible heat at the surface of the joint model earth.

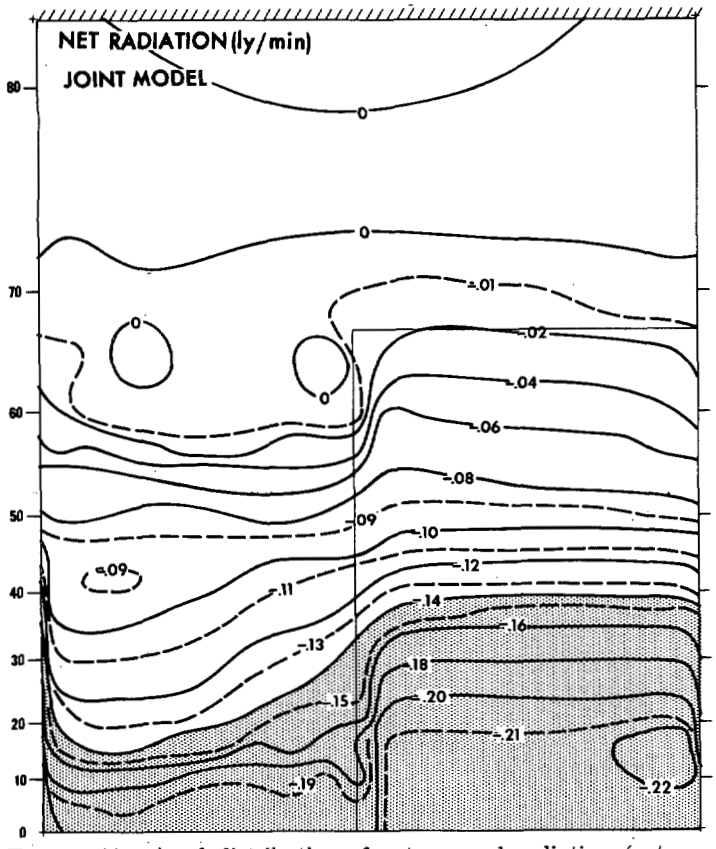

FIGURE 44.—Areal distribution of net upward radiation (net upward long-wave radiation minus net downward solar radiation) at the surface of the joint model earth.

such a way that it more closely resembles that over the actual ocean shown in figure 48 of part I.

Another component of the heat balance at the earth's surface is the net radiation (fig. 44). The distribution in the oceanic region is highly zonal. The zonal mean distribution of the net radiation at the ocean surface has already been discussed in the first part of this section.

Heat balance of the continental surface—Because the effect of advection by ocean currents does not exist over the continental areas of the joint model, heating by net radiation there must be compensated by cooling due to sensible and latent heat flux. The latitudinal distributions of zonal mean values of three heat balance components of both models are shown in figure 45. In the Tropics and middle latitudes, the turbulent flux of latent heat is the major factor in cooling the continental surface; whereas in the subtropics, the flux of sensible heat plays a major role. The latitudinal variation of soil moisture, which is described in section 8, is responsible for this result. Obviously, the rate of evaporation is very low in the continental region of the subtropics, where the amount of soil moisture is extremely small. These features of the distribution of the heat balance components are in qualitative agreement with those of the actual atmosphere obtained by Budyko (1963) and shown in figure 45B. There are, however, important differences. For example, all the heat balance components on the continental surface are extremely small poleward of about 60° latitude, but are estimated to

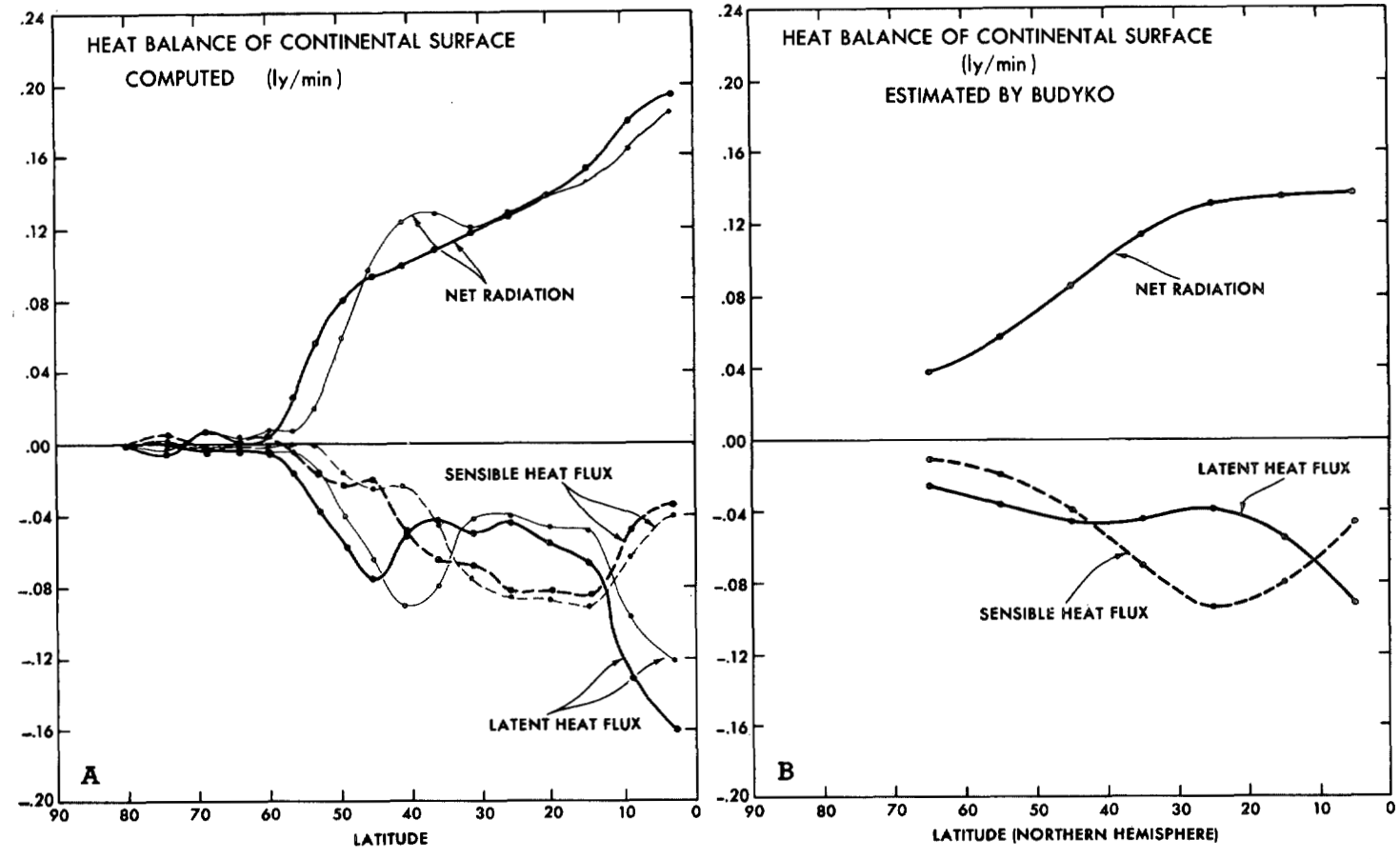

FIGURE 45.—(A) zonal mean rates of heating due to net radiation, latent heat flux, and sensible heat flux on the surface of the model continent are shown as a function of latitude; the distributions for the joint model are indicated by heavy solid lines and for the A-model by light solid lines; (B) the corresponding distributions on the surface of the actual continents as estimated by Budyko (1963).

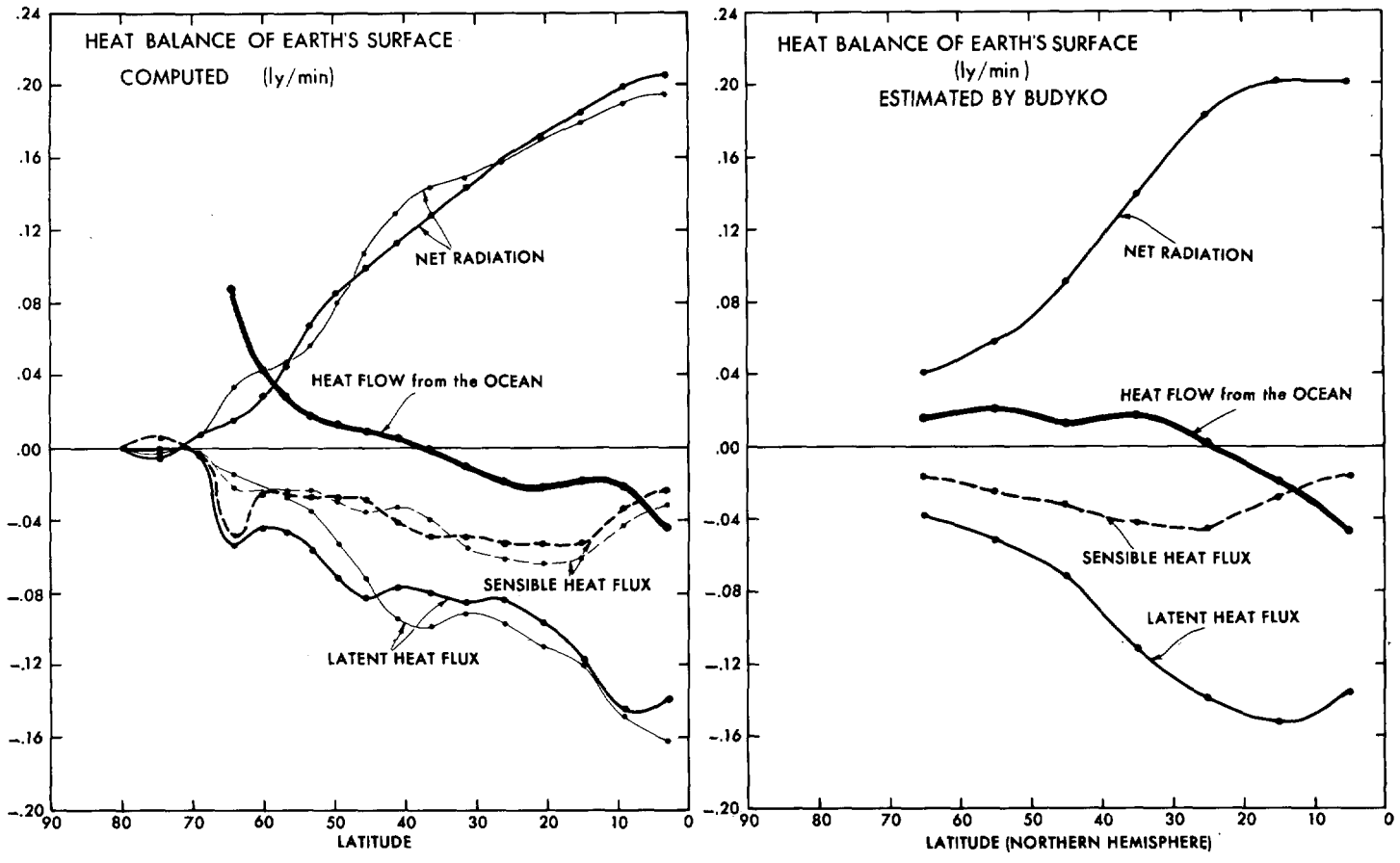

FIGURE 46.—Zonal mean rates of heating of the earth's surface (including both oceanic and continental surfaces) due to various thermal processes. For further details, see figure 41.

have significant magnitude on the actual continental surface. Though somewhat larger for the joint model than for the A-model, in both they seem to be too small. This discrepancy may be due to the excessive snow cover in the polar cap continent already discussed.

Also, the magnitudes of net downward radiation and the heat loss by evaporation in the model Tropics are significantly larger than those estimated by Budyko, probably because of the lack of longitudinal variation of cloudiness in the model atmosphere. In the actual Tropics, the Walker circulation mentioned in subsection 8A should raise the cloudiness over the continent, lower it over the ocean, and create the longitudinal variation of cloudiness. It, therefore, should suppress the downward solar radiation and, accordingly, the evaporation rate over the continent.

The areal distributions of various heat balance components on the continental surface of the joint model may be found in figures 43 and 44. One of the most notable features of these distributions is the appearance of extremely large values of sensible heat flux and extremely small values of latent heat flux in the western part of the continental region of the subtropical desert. This area of large flux of sensible heat of the joint model is more or less limited to the western half of the continent; whereas, that of the A-model extends to the eastern half (fig. 47 of part I). As discussed in section 8, this difference is caused by the modification of the rainfall pattern due to the effect of ocean circulation. Owing to the extremely high surface temperature of the desert in the western end of the continent, the net radiation shown in figure 44 has a relatively small value there.

Heat balance of the earth's surface—Having discussed the heat balance of the continental surface and that of the oceanic surface separately, we now turn to the distribution of heat balance components on the earth's surface as a whole. The latitudinal distributions for both models and those for the actual earth's surface estimated by Budyko (1963) are shown in the left and right parts of figure 46. As one would expect from the discussion of the preceding subsection, the general agreement between them is reasonably good, though the rate of latent heat flux in the subtropics of the joint model is significantly smaller than in the actual subtropics.

By comparing the distribution of heat balance components of the A-model with those of the joint model shown in figure 46, one can see how the heat balance of the earth's surface is affected by heat advection by the ocean currents. For example, it is evident that the general latitudinal gradient of the magnitude of latent heat flux is decreased significantly by this effect.

Areal mean heat balance—In table 1, the areal mean values of various heat balance components of the joint model are compared with those of the actual earth's surface estimated by Budyko (1963). The corresponding values of the A-model are included in parentheses for comparison. As this table indicates, the heat balance of

TABLE 1.—*Heat balance components of the earth's surface. The values of the joint model and those of the A-model (in parentheses) are compared with those estimated by Budyko (1963) for the actual earth's surface.*

	Whole earth	
	Model earth	Real earth
Radiation balance	0.131 (+0.132)	+0.137
Latent heat	−.088 (−.092)	−.112
Sensible heat	−.037 (−.038)	−.025
Oceanic heat flow	−.005	
	Continent	
Radiation balance	0.104 (+0.102)	+.093
Latent heat	−.061 (−.504)	−.048
Sensible heat	−.043 (−.044)	−.046
	Ocean	
Radiation balance	0.163 (+0.167)	+0.156
Latent heat	−.120 (−.136)	−.141
Sensible heat	−.030 (−.030)	−.015
Oceanic heat flow	−.010	

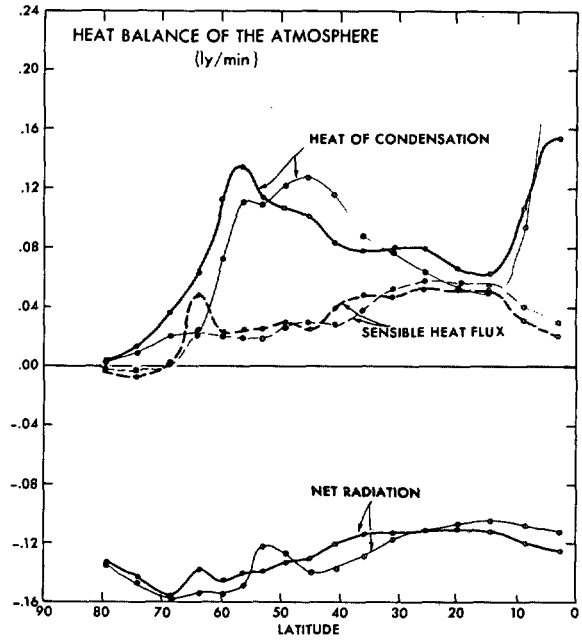

FIGURE 47.—Rates of heating of the atmosphere due to condensation, sensible heat, and net radiation (including both solar radiation and long-wave radiation) are shown as functions of latitude. Heavy lines, the distributions of the joint model; light lines, the distributions for the A-model.

the joint model surface is essentially maintained as the balance between the heat gain due to the net downward radiation and the heat loss due to the turbulent fluxes of both sensible and latent heat. In addition, there is a small loss of heat due to the net downward flow of heat from the surface to the interior of the model ocean. The existence of this net heat flow indicates that the mean temperature of the model ocean was slowly increasing with time. In other words, the joint system did not reach a state of quasi-equilibirum satisfactorily. Nevertheless, the thermal and dynamical structure of the atmosphere and the upper part of the ocean change little toward the end of the time integration, as discussed in subsection 4B. Therefore, it was decided to carry out the preliminary analysis of the results despite the continuous heat loss to the model ocean.

According to the estimate of Budyko (1963), the flux of latent heat is about 4.5 times as large as that of sensible heat at the earth's surface (whole earth); whereas, it is about 2.4 times as large at the surface of the joint model earth. This is partly due to the difference in the percentage coverage of the earth's surface by the oceanic area, where the rate of evaporation is relatively large. Two-thirds of the actual earth is covered by the sea; whereas, only 46 percent of the surface of the model earth is assumed to be covered by the oceanic area. In view of the extreme idealization of the land-sea configuration chosen for this study, it is surprising that the magnitudes of various heat balance components at the earth's surface of both models agree with those estimated for the actual earth surface as well as they do.

C. HEAT BALANCE OF THE ATMOSPHERE

The atmosphere is heated by heat of condensation and by the turbulent flux of sensible heat from the earth's surface, while it is cooled by radiation. Figure 47 shows the latitudinal distribution of these quantities in both model atmospheres. In general, the distributions of sensible heat flux and radiative cooling of the joint model are very similar to those of the A-model. However, the distribution of the heat of condensation is significantly altered by the effect of ocean currents. For example, the heat of condensation is drastically reduced in the Tropics due to the suppression of the tropical rain belt by the upwelling of cold water there; it is increased significantly in high latitudes due to the rise of the sea-surface temperature and the resulting increase of evaporation rate caused by the effect of ocean currents. These differences in the magnitude of the heat balance component affect the thermal imbalance that should be compensated by the advection of heat by atmospheric flow. Figure 48 shows the latitudinal distributions of heating due to advection. In this figure, a heavy line indicates the distribution of the joint model, and a thin line indicates the distribution of the A-model. Both models have large advective cooling in the Tropics and large advective heating in high latitudes. Owing mainly to the difference in the distribution of the heat of condensation described above, the magnitudes of the tropical advective cooling and polar advective heating of the joint model are both significantly smaller than those of the A-model. Accordingly, the poleward transport of energy in the joint model atmosphere should be significantly smaller than in the A-model atmosphere. This difference will be discussed again in the following section.

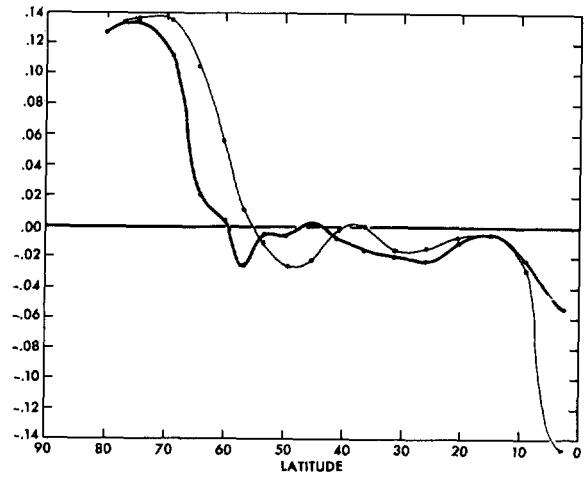

FIGURE 48.—Latitudinal distributions of heating due to the effects of advection (ly min^{-1}) in the atmosphere. Heavy line, the distribution of the joint model; light line, the distribution for the A-model.

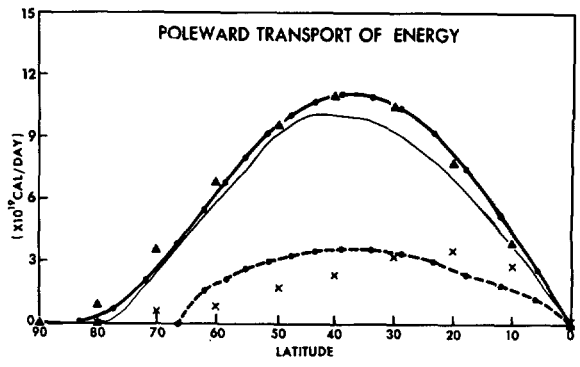

FIGURE 49.—Latitudinal distribution of the rate of the poleward transport of energy by the joint system of the model atmosphere and model ocean is shown by a heavy solid line; the corresponding quantity for the actual ocean atmosphere system, estimated by Houghton (1954) and based upon the net radiation at the top of the atmosphere, is signified by solid triangles; the rate of the poleward transport of heat by the model ocean estimated from the heat imbalance of the earth's surface is shown by a dashed line; the corresponding quantity for the actual ocean, estimated from the study of heat balance at the earth's surface by Budyko (1963), is shown by x's (average of the two hemispheres); for comparison, the poleward transport of energy by the A-model atmosphere is signified by a light line.

10. POLEWARD TRANSPORT OF ENERGY

A. POLEWARD TRANSPORT OF ENERGY BY THE JOINT SYSTEM

The rate of the poleward transport of energy by the joint ocean-atmosphere model, computed by areally integrating the net flux of radiation at the top of the model atmosphere, is shown as a function of latitude in figure 49. The distribution of the transport agrees reasonably well with that of the actual atmosphere, as estimated by Houghton (1954) and plotted in the same figure. For comparison, the distribution of the same quantity for the A-model is included in the figure (light line). The difference between the two distributions is very small. As discussed earlier, the ocean circulation mainly affects the temperature of the lower troposphere; its effect on the outgoing radiation at the top of the atmosphere is small. Accordingly, the difference between the poleward transport of energy by the joint model system and by the A-model system is much less than the magnitude of the energy transport by ocean currents, which we shall discuss here.

The latitudinal distribution of the poleward transport of heat energy by the joint model ocean is computed from the areal distribution of the heat imbalance of the ocean[5] and is shown in figure 49. The values of the heat transport by the actual ocean, computed from the estimates of the heat balance by Budyko (1963), are also plotted in the same figure for comparison. The magnitude of heat transport by the model ocean, in general, is about 25 or 30 percent of that of the joint ocean-atmosphere system and compares favorably with Budyko's estimates for the actual ocean. This agreement indicates a proper choice of the vertical thermal mixing coefficient in the model ocean, because this parameter controls the intensity of the poleward transport of heat by ocean currents (Bryan, 1967, for example). Further examination of the results, however, reveals that the rate of transport by the model ocean is smaller at low latitudes and is larger at high latitudes than that estimated for the actual ocean. In other words, the latitude of maximum energy transport in the joint model ocean is higher than in the actual ocean, estimated from Budyko's results. As pointed out in section 8, the rates of evaporation from the subtropical region of the joint model ocean are less than from the corresponding regions of the actual ocean surface. Also, the turbulent fluxes of both sensible and latent heat from the subarctic ocean of the joint model are much larger than those from the corresponding area of the actual ocean surface (see subsection 9B). These decrepancies in energy flux from the ocean to the atmosphere are consistent with discrepancies in the latitude of maximum poleward transport of heat energy by ocean currents mentioned above.

B. POLEWARD TRANSPORT OF ENERGY BY THE ATMOSPHERE

In figure 49, the difference between the poleward transport of energy by the joint ocean-atmosphere system and by the ocean represents the transport of energy by the atmosphere, which is about twice as large as that of the ocean. As pointed out in the previous subsection, the magnitude of the poleward transport of heat energy expected from the net radiative flux at the top of the atmosphere is affected slightly by the ocean circulation. Accordingly, the difference between the energy transport in the joint model atmosphere and in the A-model atmosphere is almost as much as the magnitude of the oceanic heat transport. The transport in the joint model atmosphere is accomplished by two processes: 1) the transport of heat energy [6] and 2) the transport of latent energy. In figure 50, the latitudinal distributions of

[5] As mentioned in the previous section, the area integral of heat imbalance is not equal to zero because of the net inflow of heat from the surface to the interior of the model ocean. Therefore, it is necessary to normalize the values of heat imbalance in order to evaluate the poleward transport of heat energy shown in figure 49. See part III for the exact value of heat transport by the model ocean.

[6] Heat energy $=c_pT+\phi+K$ where c_p is the specific heat of air under constant pressure. T, ϕ, and K are temperature, geopotential height, and kinetic energy.

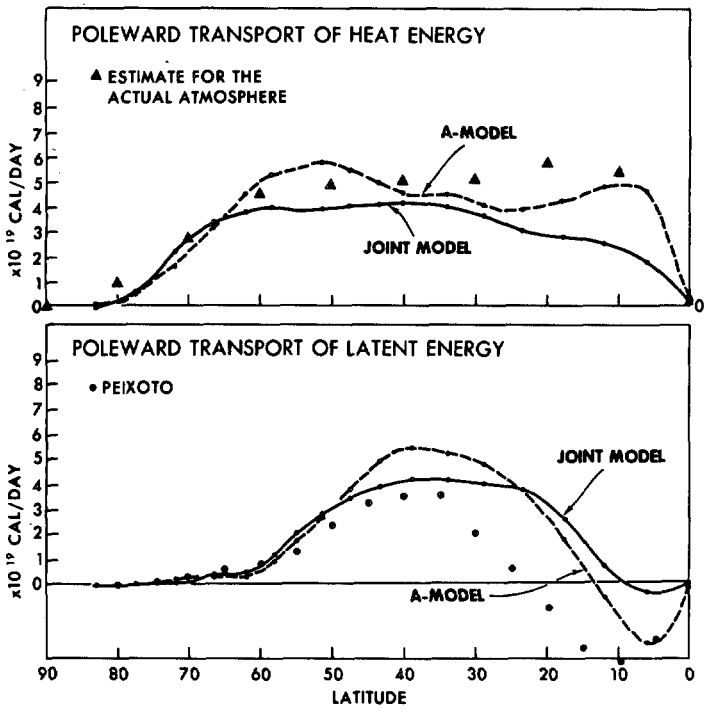

FIGURE 50.—Latitudinal distributions of poleward transport of heat energy ($c_pT+\phi+K$) and latent energy in the joint model atmosphere and in the A-model atmosphere are shown by solid and dashed lines, respectively. The solid triangles indicate the values of the heat energy transport estimated from the heat balance computation of Houghton (1954) and Budyko (1963). The heavy dots in the lower diagram indicate the poleward transport of latent energy estimated by Peixoto and Crisi (1965).

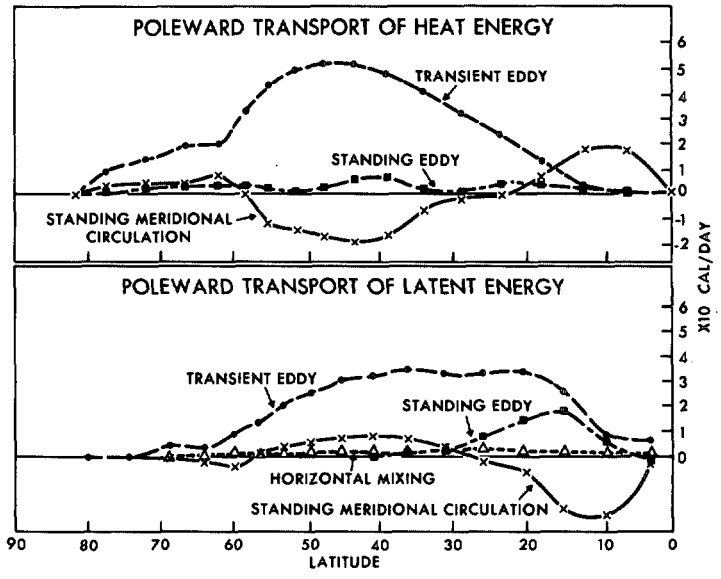

FIGURE 51.—Latitudinal distributions of the poleward transport of heat energy and latent energy in the joint model atmosphere due to standing meridional circulations, transient eddies, standing eddies, and subgrid scale horizontal mixing.

poleward transport of heat energy and of latent energy in both the joint model atmosphere and the A-model atmosphere are shown. In low latitudes, the equatorward transport of latent energy and the poleward transport of heat energy in the joint model atmosphere are much smaller than those in the A-model atmosphere. This difference is again due to the suppression of the direct Hadley cell by the cold sea-surface temperature at the Equator of the joint model. If one compares the distribution of the meridional transport of latent energy in the joint model atmosphere with its counterpart in the actual atmosphere, obtained by Peixoto and Crisi (1965) and plotted in figure 50, he will notice that the equatorial transport of the moisture in the former is much less extensive than in the latter. This result is consistent with the fact that the tropical rain belt of the joint model is narrower and weaker than the tropical rain belt determined from the annual mean rainfall in the actual atmosphere (fig. 33). As discussed in subsection 8A, the lack of the seasonal variation of solar radiation and, accordingly, the lack of the seasonal variation of the location of the tropical rain belt should partly be responsible for this difference.

In middle latitudes, the poleward transports of both heat energy and latent energy in the joint model atmosphere are somewhat smaller than those in the A-model atmosphere. The poleward transport of heat energy of the model ocean decreases the magnitude of the meridional gradient of temperature in the middle latitude and, thus, of eddy kinetic energy in the joint model atmosphere. This point was discussed in section 3. The reduction of both eddy kinetic energy and meridional temperature gradient is obviously responsible for the decrease of the poleward transport of energy in middle latitudes associated with atmospheric circulation.

In figure 51, the poleward transport of heat energy and latent energy in the joint model atmosphere is further broken down into the following components: 1) transport by transient eddies, 2) transport by standing eddies, 3) transport by standing meridional circulation, and 4) transport by subgrid scale eddies. The definitions of these components of transport may be found in subsection 5B of part I. One can compare figure 51 with figure 38 of part I, showing the distribution of the corresponding transports in the A-model atmosphere. In this comparison, it is evident again that the transports by the direct tropical cell are drastically reduced as a result of the low sea-surface temperature at the Equator. Also, the magnitudes of transports by transient eddies in middle latitudes are significantly reduced due to the oceanic transport of heat energy.

11. SUMMARY AND CONCLUSIONS

By comparing the state of the joint model atmosphere with the state of the A-model atmosphere, we have tried to identify various influences of the circulation of the model ocean on the general circulation and the hydrologic cycle of the model atmosphere. We shall list some of these effects.

1) The poleward transport of heat by the ocean circulation decreases the poleward transport of heat energy and latent energy in the atmosphere; it also decreases the meridional temperature gradient of the atmosphere, particularly in the lower troposphere. Accordingly, the intensity of the zonal wind and of the vertical wind shear decreases, and the atmosphere becomes more stable with respect to baroclinic disturbances. Thus, the general level of eddy kinetic energy in the middle-latitude region is lowered, and the intensity of the indirect cell of meridional circulation decreases.

2) In middle and high latitudes, the increase in the temperature contrast between the ocean and the continent accentuates the longitudinal variation of eddy kinetic energy. In other words, the oceanic heating of the cold continental air tends to enhance the development of cyclones off the east coast of the continent in higher latitudes.

3) Examination of the distributions of the zonal mean surface pressure indicated that the intensity of the subtropical High, the middle latitude Low, and the polar High becomes less pronounced as a result of the ocean circulation. The resulting decrease in intensity of the zonal current at the earth's surface lowers the level of the exchange of angular momentum between the atmosphere and the earth's surface. Therefore, the magnitude of the meridional transport of angular momentum is significantly smaller as a result of the influence of the ocean circulation.

4) At the Equator, the upwelling of relativity cold water tends to suppress the intensity of the tropical rainfall in the oceanic region. This suppression results in the general weakening of the direct meridional circulation cell in the Tropics and drastically cuts down the magnitude of equatorward transport of moisture and the poleward transport of heat energy by this cell.

5) This equatorial belt of low sea-surface temperature also helps maintain the zonal circulation in the vertical zonal plane on the Equator. This circulation consists of surface easterlies, upper air westerlies, downward motion in the eastern part of the ocean, and upward motion in the eastern part of the continent. It supplies the moisture from ocean to continent and significantly increases the amount of rainfall and runoff in the continental region of the Tropics.

6) In the subtropics and the middle-latitude region, the advection of warm water by the subtropical gyre increases the supply of sensible and latent heat from the ocean to the atmosphere along the east coast of the continent. This, in turn, increases the rainfall in this region and in the eastern part of the continent and limits the subtropical desert to the western half of the continent.

7) In higher latitudes, the advection of warm water by the subarctic gyre increases the flux of both sensible and latent heat off the west coast of the continent near 55° latitude. This supply of energy, in turn, increases the intensity of precipitation in this area. The middle-latitude rain belt shifts, in general, poleward due to the effect of the ocean currents.

8) The ocean circulation contributes to the poleward retreat of the snow boundary. Nevertheless, the accumulation of snow takes place poleward of 58° latitude. Thus, the intense polar High remains, despite the effect of the ocean.

9) About two-thirds of the poleward transport of heat is accomplished by the circulation in the model atmosphere and the remaining one-third by the currents in the model ocean.

Though there are some exceptions, the features of the joint model atmosphere are, in general, more realistic than those of the A-model. Therefore, it is highly probable that the various effects of the circulation of the model ocean identified in this study are also influencing the actual climate.

12. IMPROVEMENT OF THE MODEL

There are many features of the model that require further improvement. As the discussions in part III indicate, the deeper part of the ocean did not reach the state of thermal equilibrium during the period of the time integration. The small net downward flow of heat from the surface to the interior of the model ocean, which produces a slow rise in the deep sea temperature, could affect the climate in the model atmosphere. It is, therefore, very desirable to improve the method of approach and to obtain a state sufficiently close to the state of so-called "quasi-equilibrium."

One of the important factors not considered in this study is the seasonal variation of the solar radiation. After completion of the present study, time integration of the joint model with the seasonal variation was accomplished. The preliminary results from this new study indicate that this effect markedly alters the climate of the joint model atmosphere. Particularly, the temperature of the earth's surface in higher latitudes is increased significantly as a result of the seasonal variation of the solar radiation.

Another important factor missing from the joint model is the radiation-hydrology coupling. In order to minimize the risk of getting too unrealistic a model atmosphere, we computed the radiative transfer by using the zonal mean of the climatological distribution of water vapor in the actual atmosphere instead of the distribution obtained from the hydrologic part of the model. In other words, the present model does not have a direct coupling between radiative transfer and the hydrologic cycle. A study by Manabe and Wetherald (1967) suggests that this coupling almost doubles the sensitivity of the temperature of the model atmosphere to a change in the solar constant. It is probable that the incorporation of this coupling into the model could increase significantly the influence of ocean currents upon the model climate.

Further improvements of high-speed computers may enable us to construct and integrate a joint ocean-atmosphere model with a realistic land-sea distribution. Then, one will be able to discuss the climatology of the earth's atmosphere on a quantitative basis.

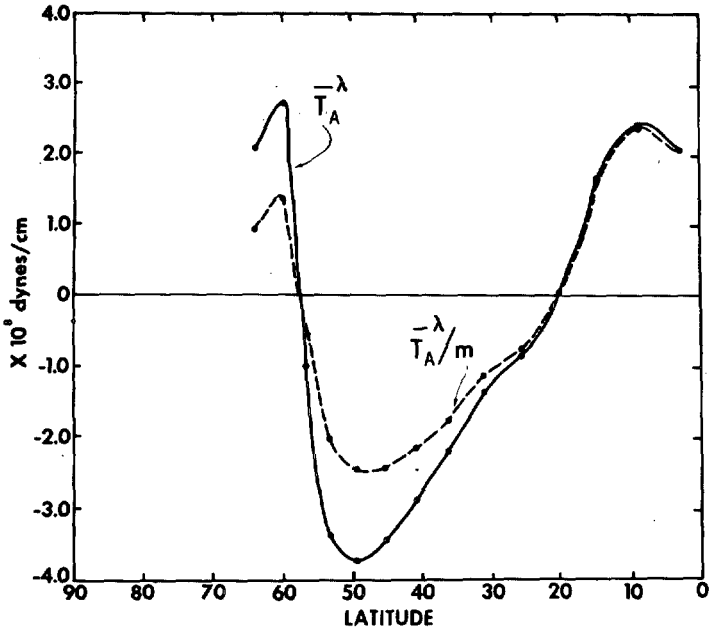

FIGURE 52.—Latitudinal distributions $\overline{T_A}^{\lambda}$ and $\overline{T_A}^{\lambda}/m$.

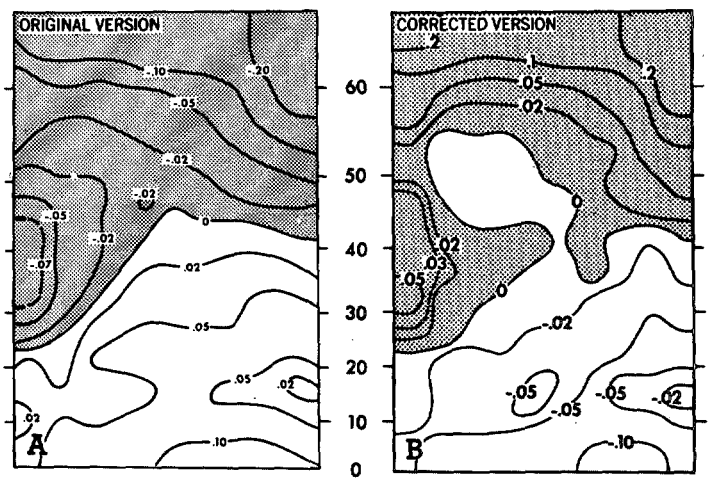

FIGURE 53.—Areal distributions of heat flow from the interior to the surface of the ocean in units of ly min^{-1}; (A) the distribution of the original joint model; and (B) the distribution of the corrected joint model obtained by taking the time average for the last 30 atmospheric days of the integration of the corrected model.

APPENDIX

As mentioned briefly in section 2, the joint ocean-atmosphere model described thus far has a code error in the part of the program dealing with the exchange of wind stress between the ocean and atmosphere. The torque exerted on the lower boundary of the atmosphere, T_A, and the torque exerted on the ocean surface, T_0, should have the following relationship:

$$T_0 = -T_A.$$

Instead, the following relationship holds as a result of the code error:

$$T_0 = -T_A/m$$

where m denotes the magnification factor of the Mercator projection. Figure 52 shows the distributions of the zonal mean values of $\overline{T_A}^{\lambda}$ and $\overline{T_A}^{\lambda}/m$ on the ocean surface. After detecting this code error, the time integration of the model was extended for 30 more oceanic years or about 100 more atmospheric days. In the original integration, both the total kinetic energy and the variance of the zonal mean sea-surface temperature, which is an indicator of the meridional temperature gradient of the ocean surface, underwent most of its time change during the first 100 atmospheric model days of the integration. Therefore, this period of extension was chosen so that the major adjustment in the atmospheric circulation and in the temperature distribution in the upper part of the ocean could be accomplished during this time period.

As we have demonstrated earlier, the heat flow from the interior to the surface of the ocean controls the influence of the ocean on the heat balance and hydrology of the atmosphere and is the most fundamental quantity of the ocean-atmosphere interaction. In figure 53, the distribution of this heat flow of the original model is compared with

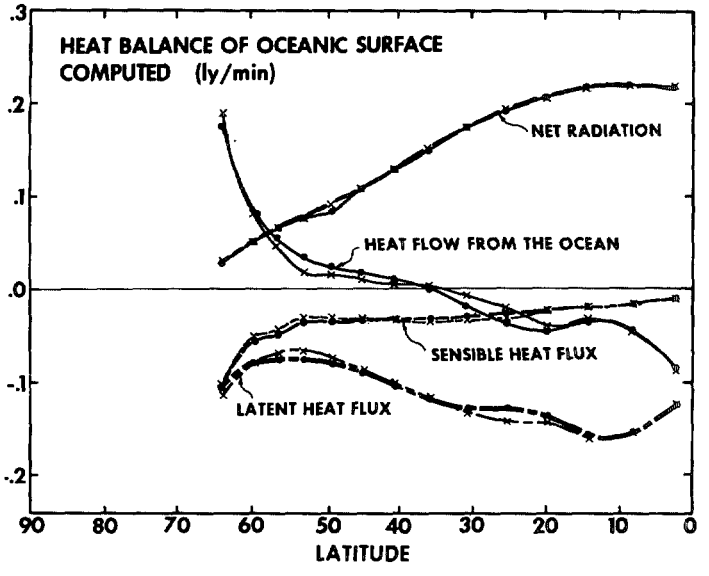

FIGURE 54.—Zonal mean rates of heating of the ocean surface due to net radiation, latent heat flux, sensible heat flux, and the heat flow from the interior to the surface of the model ocean. The distributions of the original joint model and of the corrected joint model are shown by heavy and light lines, respectively.

that of the corrected model. The latter is obtained by taking the time mean for the last 30 atmospheric days of the extended integration. In this comparison, there are some differences. For example, the distribution of the corrected model has a belt of weak negative heat flow between the area of strong heating along the east coast of the continent (35° latitude) and along the west coast of the continent (60° latitude). This feature probably resulted from the intensification of the subarctic gyre due to the correction of the code error and is missing in the distribution of the original model. The general features of the two distributions, however, are very similar.

Figure 54 was constructed in order to evaluate quantitatively the difference in the distribution of the various

heat balance components on the ocean surface. In this figure, the latitudinal distributions of zonal mean values of net radiation, sensible heat flux, latent heat flux, and heat flow from the interior to the surface of the model ocean are shown. Light lines and heavy lines indicate the distributions of the original model and of the corrected model, respectively. In this comparison, the differences between the two versions are very small indeed. Therefore, we retained the results from the original model in the preceding section and did not replace them by the results from the corrected model.

ACKNOWLEDGMENTS

This study is the result of a collaborative project with Dr. Kirk Bryan. It has been a great pleasure to be able to work with him.

The author wishes to thank Mr. J. Leith Holloway, Jr., who directed the construction of the computer program of the joint model and made valuable suggestions on the use of the exponential filter described in section 3.

The author is very grateful to Dr. Joseph Smagorinsky, Director of the Geophysical Fluid Dynamics Laboratory, ESSA, for a number of valuable suggestions and for constant encouragement so vital to a project of this sort.

Thanks are due Mr. Richard T. Wetherald who completed the computer program of the hydrological processes.

REFERENCES

Bjerknes, J., "Atmospheric Teleconnections From the Equatorial Pacific," *Monthly Weather Review*, Vol. 97, No. 3, Mar. **1969**, pp. 163–172.

Bryan, K., "Climate and the Ocean Circulation: III. The Ocean Model," *Monthly Weather Review*, Vol. 97, No. 11, Nov. **1969**, pp. 806–827.

Bryan, K., and Cox, M., "A Numerical Investigation of the Oceanic General Circulation," *Tellus*, Vol. 19, No. 1, Feb. **1967**, pp. 54–80.

Buch, H. S., "Hemispheric Wind Conditions During the Year 1950," *Final Report*, Part 2, Contract No. AH19–122–153, Department of Meteorology, Massachusetts Institute of Technology, Cambridge, **1954**, 126 pp.

Budyko, M. I., "Teplovĭ balans zemnoĭ poverkhrosti," (Heat Balance of the Earth's Surface), Gidrometeoizdat, Leningrad, **1956**, 255 pp.

Budyko, M. I., (Editor), *Atlas Teplovo Balansa Zemnogo Shara* (Guide to the Atlas of the Heat Balance of the Earth), Gidrometeoizdat, Moscow, **1963**, 69 pp.

Holloway, J. L., Jr., "Smoothing and Filtering of Time Series and Space Fields," *Advances in Geophysics*, Vol. 4, Academic Press, Inc., New York, **1958**, pp. 351–390.

Houghton, H. G., "On the Annual Heat Balance of the Northern Hemisphere," *Journal of Meteorology*, Vol. 11, No. 1, Jan. **1954**, pp. 1–9.

London, J., "A Study of the Atmospheric Heat Balance," *Final Report*, Contract No. AF19(122)–165, Department of Meteorology and Oceanography, New York University, July **1957**, 99 pp.

Lvovitch, M. I., and Ovtchinnikov, S. P., "River Drainage," *Physical-Geographical Atlas of the World*, Akademy of Sciences SSSR and Central Administration of Geodesy and Cartography of USSR, Moscow, **1964**, 289 pp. (see pp. 60–61).

Manabe, S., "Climate and the Ocean Circulation: I. The Atmospheric Circulation and the Hydrology of the Earth's Surface," *Monthly Weather Review*, Vol. 97, No. 11, Nov. **1969**, pp. 739–774.

Manabe, S., and Wetherald, R. T., "Thermal Equilibrium of the Atmosphere With a Given Distribution of Relative Humidity," *Journal of the Atmospheric Sciences*, Vol. 24, No. 3, May **1967**, pp. 241–259.

Manabe, S., and Smagorinskv, J., "Simulated Climatology of a General Circulation Model With a Hydrologic Cycle: II. Analysis of the Tropical Atmosphere," *Monthly Weather Review*, Vol. 95, No. 4, Apr. **1967**, pp. 155–169.

Manabe, S., Smagorinsky, J., Holloway, J. L., Jr., and Stone, H. M., "Simulated Climatology of a General Circulation Model With a Hydrologic Cycle: III. Improvement of Horizontal Resolution of Finite Difference," *Monthly Weather Review*, Vol. 98, **1970**, (to be published).

Öpik, E. J., "Convective Transfer in the Problem of Climate," *Geophysical Bulletin* No. 8, Institute for Advanced Studies, School of Cosmic Physics, Dublin, Oct. **1953**, 14 pp.

Panofsky, H. A., and Brier, G. W., *Some Applications of Statistics to Meteorology*, College of Mineral Industries, The Pennsylvania State University, University Park, **1958**, 224 pp.

Peixoto, J. P., and Crisi, A. R., "Hemispheric Humidity Conditions During the IGY," *Scientific Report* No. 6, Contract No. AF19(628)–2408, Department of Meteorology, Massachusetts Institute of Technology, Cambridge, Nov. **1965**, 166 pp.

Priestley, C. H. B., "A Survey of the Stress Between the Ocean and the Atmosphere," *Australian Journal of Scientific Research*, Ser. A, Vol. 4, No. 3, Sept. **1951**, pp. 315–328.

Saltzman, B., and Fleisher, A., "Spectral Statistics of the Wind at 500 Mb.," *Journal of the Atmospheric Sciences*, Vol. 19, No. 2, Mar. **1962**, pp. 195–204.

Taylor, V. R., and Winston, J. S., "Monthly and Seasonal Mean Global Charts of Brightness From ESSA 3 and ESSA 5 Digitized Pictures, February 1967–February 1968," *ESSA Technical Report* NESC 46, National Environmental Satellite Center, Washington, D.C., Nov. **1968**, 9 pp. plus charts.

Troup, A. J., "The Southern Oscillation," *Quarterly Journal of the Royal Meteorological Society*, Vol. 91, No. 390, Oct. **1965**, pp. 490–506.

Wetherald, R. P., and Manabe, S., "Response of the Joint Ocean-Atmosphere Model to the Seasonal Variation of the Solar Radiation," Geophysical Fluid Dynamics Laboratory, ESSA, Princeton, N.J., **1969**, (unpublished results).

[Received February 3, 1969; revised June 9, 1969]